


# YY1 regulates skeletal muscle regeneration through controlling metabolic reprogramming of satellite cells

Fengyuan Chen<sup>1</sup>, Jiajian Zhou<sup>2</sup>, Yuying Li<sup>2</sup>, Yu Zhao<sup>1</sup>, Jie Yuan<sup>2</sup>, Yang Cao<sup>2</sup>, Lijun Wang<sup>1</sup>, Zongkang Zhang<sup>3</sup>, Baoting Zhang<sup>3</sup>, Chi Chiu Wang<sup>4</sup>, Tom H Cheung<sup>5</sup>, Zhenguo Wu<sup>5</sup> , Carmen Chak-Lui Wong<sup>6</sup>, Hao Sun<sup>2,\*</sup>  & Huating Wang<sup>1,\*\*</sup> 

## Abstract

Skeletal muscle satellite cells (SCs) are adult muscle stem cells responsible for muscle regeneration after acute or chronic injuries. The lineage progression of quiescent SC toward activation, proliferation, and differentiation during the regeneration is orchestrated by cascades of transcription factors (TFs). Here, we elucidate the function of TF Yin Yang1 (YY1) in muscle regeneration. Muscle-specific deletion of YY1 in embryonic muscle progenitors leads to severe deformity of diaphragm muscle formation, thus neonatal death. Inducible deletion of YY1 in SC almost completely blocks the acute damage-induced muscle repair and exacerbates the chronic injury-induced dystrophic phenotype. Examination of SC revealed that YY1 loss results in cell-autonomous defect in activation and proliferation. Mechanistic search revealed that YY1 binds and represses mitochondrial gene expression. Simultaneously, it also stabilizes Hif1 $\alpha$  protein and activates Hif1 $\alpha$ -mediated glycolytic genes to facilitate a metabolic reprogramming toward glycolysis which is needed for SC proliferation. Altogether, our findings have identified YY1 as a key regulator of SC metabolic reprogramming through its dual roles in modulating both mitochondrial and glycolytic pathways.

**Keywords** Hif1 $\alpha$ ; metabolic reprogramming; muscle satellite cell; skeletal muscle regeneration; YY1

**Subject Categories** Metabolism; Stem Cells; Transcription

**DOI** 10.15252/embj.201899727 | Received 29 April 2018 | Revised 17 December 2018 | Accepted 19 December 2018 | Published online 12 April 2019

**The EMBO Journal (2019) 38: e99727**

## Introduction

Skeletal muscle has a robust regenerative capacity, with rapid reestablishment of full power occurring even after severe damage that causes widespread myofiber necrosis. The cells responsible for muscle regeneration are resident muscle stem cells, also called satellite cells (SCs) which are located in a niche beneath the ensheathing basal lamina on the surface of the myofibers and maintained in a quiescent stage (Aziz *et al*, 2012; Bentzinger *et al*, 2012; Relaix & Zammit, 2012). Most satellite cells in postnatal muscles originate from a population of embryonic precursors that express paired box protein 7 (Pax7) and/or the related Pax3. These cells are of mesodermal origin and arise from a dorsal structure of the developing somite (known as the dermomyotome). Under the control of Pax3, the cells delaminate from the ventrolateral lips of the dermomyotome and migrate to the sites of limb and diaphragm to provide myogenic progenitor cells at these sites. In mouse, during fetal stages E12.5–E17.5, the level of Pax3 protein is reduced, accompanied by the appearance of Pax7<sup>+</sup> progenitors contributing to the formation of fetal myofibers and establishment of the major source of postnatal satellite cells (Buckingham, 2007; Buckingham & Relaix, 2007; Bentzinger *et al*, 2012). Upon injury in adult muscle, SCs are rapidly activated, undergo proliferative expansion, and eventually differentiate and fuse to form new myofibers (Aziz *et al*, 2012; Bentzinger *et al*, 2012; Relaix & Zammit, 2012). A subset of SCs undergoes self-renewal and return to quiescent state to replenish the adult stem cell pool. SCs are inextricably linked to Pax7 which is expressed and maintained in virtually all quiescent SCs in adult mouse muscles (Seale *et al*, 2000; Buckingham, 2007; Buckingham & Relaix, 2007), thus provides a valuable target locus to facilitate genetic manipulation of the SC genome.

1 Department of Orthopedics and Traumatology, Li Ka Shing Institute of Health Sciences, Chinese University of Hong Kong, Hong Kong, China

2 Department of Chemical Pathology, Li Ka Shing Institute of Health Sciences, Chinese University of Hong Kong, Hong Kong, China

3 School of Chinese Medicine, Faculty of Medicine, The Chinese University of Hong Kong, Hong Kong, China

4 Department of Obstetrics and Gynecology, Li Ka Shing Institute of Health Sciences, The Prince of Wales Hospital, The Chinese University of Hong Kong, Hong Kong, China

5 The State Key Lab in Molecular Neuroscience, Division of Life Science, Center for Stem Cell Research and Center for Systems Biology and Human Diseases, The Hong Kong University of Science and Technology, Hong Kong, China

6 Department of Pathology, The University of Hong Kong, Hong Kong

\*Corresponding author. Tel: +852 37636048; E-mail: haosun@cuhk.edu.hk

\*\*Corresponding author. Tel: +852 37636047; E-mail: huating.wang@cuhk.edu.hk

In the process of regeneration, activation of SCs following muscle injury results in the expansion of myogenic cell pool and leads to the initiation of myogenic program. This program, orchestrated by a regulated cascade of myogenic regulatory factors (MRFs) including MyoD, Myf5, myogenin, and MRF4, together with Pax3 and Pax7, drives the myogenic lineage progression (Aziz *et al*, 2012; Bentzinger *et al*, 2012). Besides MRFs, the intrinsic complexity of myogenesis arises also from hierarchical interactions between transcriptional regulators, regulatory RNAs, and chromatin-remodeling factors. Yin Yang1, YY1, is a ubiquitously expressed TF which regulates various processes of development and differentiation (Gordon *et al*, 2006). Previous work from our group and others identified YY1 as an epigenetic repressor of multiple muscle genes and muscle relevant miRNAs/lincRNAs during myoblast differentiation into myotube (Wang *et al*, 2007, 2008; Lu *et al*, 2012, 2013; Zhou *et al*, 2012a). Deregulation of the YY1-regulated molecular circuitries leads to aberrant myogenic differentiation, which contributes to pathogenesis of muscle diseases including rhabdomyosarcoma and Duchenne muscular dystrophy (DMD; Wang *et al*, 2008, 2012; Zhou *et al*, 2012a). Altogether, these studies performed mainly on C2C12 myoblast cell line highlight the importance of YY1 in myoblast differentiation and underscore a need to determine the full spectrum of YY1 function in SC lineage progression and *in vivo*.

Beside the transcriptional control, metabolic control is emerging as a key regulatory mechanism of SC fate transition. Increasing evidence demonstrates that SC functions are largely controlled by two major metabolic states of the cell: oxidative (occurring in the mitochondria) and glycolytic (occurring in the cytoplasm; Garcia-Prat *et al*, 2017). Glycolysis is the enzymatic conversion of glucose to pyruvate, which generates two net ATP molecules per molecule of glucose. In contrast, cells in oxygen-rich environments can use oxidative phosphorylation (OXPHOS) for more efficient ATP production, which nets an average of 34 additional ATP molecules per glucose by oxidizing pyruvate to acetyl coenzyme A (Acetyl-CoA), then to carbon dioxide and water in the mitochondrial tricarboxylic acid (TCA) cycle. As a major location of energy production, mitochondria play a fundamental role in cell metabolism, and its function is therefore subject to tight quality control. Outstanding questions relevant to SCs include the metabolic status of quiescent satellite cells (QSCs) and how metabolism controls the transition of QSC to activated and differentiated states. Recent evidence indicates that QSCs have mitochondrial activity probably due to the aerobic SC niche, and their activation into more committed progenitors is accompanied by an increased usage of glycolytic pathway (Ryall *et al*, 2015). This so-called Warburg metabolism (aerobic glycolysis) originally discovered in cancer cells is believed to allow SCs to respond to the rapid increase in energy demand that characterizes the activated state; it also provides glycolytic intermediates which are chemical building blocks that are critical for synthesis of amino acids, lipids, and nucleic acids, which is important for SCs that need to continually replicate and divide. The metabolic reprogramming has been observed in many stem cells (Ryall *et al*, 2015). For example, emerging lines of evidence suggest that metabolic reprogramming is required at each step of the conversion of differentiated cells such as fibroblasts to iPSCs and the subsequent conversion to differentiated cells such as neurons (Gibson & Thakkar, 2018). Thus, metabolic reprogramming is not just passive bystanders but may

modulate stemness, cell differentiation, and reprogramming. Nevertheless, our knowledge of metabolic programming in SC is incomplete; how SCs achieve the successful use of glycolysis during their activation remains unclear and becomes a focus of this investigation.

In this study, utilizing several genetic mouse models, we initiated a thorough analysis of YY1 function in skeletal muscle development and regeneration. Conditional deletion of YY1 in Pax7 expressing cells led to failure of diaphragm muscle development, thus the neonatal death. Inducible deletion of YY1 in SCs severely impaired the process of acute injury-induced muscle regeneration. Moreover, deletion of YY1 in a dystrophic mdx mouse exacerbated the chronic injury-induced dystrophic phenotype. Further examination revealed the YY1 deletion resulted in cell-autonomous defect in SC activation and proliferation, pointing to YY1 as a key regulator of SC expansion. In search for molecular mechanisms underlying the above phenotypes, global profiling of YY1 regulated transcriptome and binding events revealed that during SC activation YY1 binds and directly represses mitochondrial gene expression; simultaneously, it also stabilizes Hif1 $\alpha$  protein to activate Hif1 $\alpha$ -mediated glycolytic genes. Loss of YY1 led to up-regulation of mitochondrial genes and inhibited glycolysis, thus causing the defect in SC activation. Altogether, our findings have identified YY1 as a key regulator of SC metabolic reprogramming through its dual roles in modulating both mitochondrial and glycolytic pathways.

## Results

### Conditional deletion of YY1 in muscle progenitor cells causes defect in muscle development

Constitutive ablation of YY1 in mice results in peri-implantation lethality (Donohoe *et al*, 1999). To investigate the roles of YY1 in SC function and muscle regeneration, YY1 was selectively ablated in Pax7-derived cells by crossing Pax7<sup>Cre</sup> knock-in mice expressing Cre recombinase from the Pax7 locus (Pax7<sup>Cre</sup>; Keller *et al*, 2004) with mice bearing floxed YY1 alleles (Fig EV1A, exon 1 is flanked by loxP sites; YY1<sup>f/f</sup>; Affar el *et al*, 2006). Conditional knock out allele, Pax7<sup>Cre/+</sup>; YY1<sup>f/f</sup> (thereafter referred to as YY1<sup>CKO</sup>), and control (Ctrl), Pax7<sup>+/+</sup>; YY1<sup>f/+</sup> littermates, were produced in F2 generation and used for the study (Fig 1A). We first confirmed the successful deletion of YY1 in YY1<sup>CKO</sup> by staining for both Pax7 and YY1 in the embryos. As reported before (Donohoe *et al*, 1999), YY1 is ubiquitously expressed and relatively elevated in somite, limb bud, and tail tip. At E12.5 day, there was already a complete deletion of YY1 in Pax7<sup>+</sup> cells in myotome by immunofluorescence (IF) staining (merging of Pax7/red with YY1/green in Ctrl yielded yellow cells, which were rarely found in YY1<sup>CKO</sup>; Fig 1B). When examining limb buds (Fig 1C), the majority of cells in YY1<sup>CKO</sup> appeared red; a few were yellow probably because Pax7 was not fully activated in these cells yet (Pax7 does not express in limb bud until ~E11.5; Hutcheson *et al*, 2009). Unexpectedly, YY1<sup>CKO</sup> mice died soon after birth even though they were only slightly smaller than the Ctrl and heterozygous (Het, Pax7<sup>Cre/+</sup>; YY1<sup>lox/+</sup>) mice and showed no overt morphological deformity (Figs 1D and EV1B). These pups appeared unable to breathe despite frequent gasping

and died within an hour after birth, which prompted us to examine their lungs. Indeed, postmortem analysis indicated that the lungs were not able to fill with air, thus sank in water (Fig 1E); histological examination revealed collapsed alveoli (Fig 1F), confirming that the lungs failed to inflate at birth. Since diaphragm (Dp) muscle is critical for the opening of newborn lung (Borensztein *et al*, 2013; Merrell & Kardon, 2013) and Pax7<sup>+</sup> muscle progenitors are important for Dp muscle development (Babiuk *et al*, 2003; Merrell & Kardon, 2013), we suspected there may be a defect in Dp muscle formation resulting from the YY1 deletion in Pax7<sup>+</sup> progenitors. Indeed, the YY1<sup>CKO</sup> Dp muscle appeared much thinner (Fig 1G), containing markedly reduced MyHC<sup>+</sup> muscle fibers visualized by hematoxylin and eosin (H&E) and immunohistochemistry (IHC) staining on multiple pairs of littermate embryos (E18.5 day; Fig 1H). IF staining with MyHC and troponin T proteins also confirmed the massive loss of muscle fibers in the YY1<sup>CKO</sup> Dp (Fig 1I and J). Further examining the limb muscles which are also developed from Pax7<sup>+</sup> progenitors, we found the basic pattern of hindlimb muscles was present in P0 YY1<sup>CKO</sup> mice, but each muscle appeared slightly smaller and the number of MyHC<sup>+</sup> or TnT<sup>+</sup> fibers was also decreased (52 and 54%) compared to Ctrl littermates (Fig 1K–M) while the size of myofibers (measured by cross-sectional area, CSA) was increased (Fig EV1C). These results suggested the deletion of YY1 in Pax7-expressing muscle progenitors causes a defect in body/limb muscle formation, highlighting a critical need for YY1 during embryonic/fetal muscle development. To further test this notion, we examined the progenitor cells along developmental stages. At the early embryonic stage (E12.5 day), staining for Pax7 or MyoD did not reveal obvious reduction in the number of progenitors in myotome, nor was there any evident defect in the myotome structure (Fig EV1D). However, when examined at days E14.5 (Fig EV1E) and E18.5 (Figs 1N and EV1F), a marked decrease in the number of Pax7<sup>+</sup> (35%) or MyoD<sup>+</sup> (39%) cells was found in the limb muscle. Similarly, the number of Pax7<sup>+</sup> cells was also reduced in the Dp muscle of iKO vs. Ctrl mouse (Fig 1O). Altogether, the above results suggested YY1 plays a critical role in muscle development and the expansion of Pax7<sup>+</sup> progenitor pool during embryonic/fetal myogenesis.

### Inducible ablation of YY1 in adult muscle severely hampered injury-induced muscle regeneration

To circumvent the developmental defect and neonatal death, we next employed an inducible Cre driver in which tamoxifen (TM)-inducible CreER protein is expressed from a modified Pax7 locus, Pax7<sup>CreERT2</sup> (Lepper *et al*, 2009). Mice with the Pax7<sup>CreERT2/+</sup> allele were crossed to YY1<sup>f/f</sup> mice, to generate Pax7<sup>CreERT2/+</sup>;YY1<sup>f/f</sup> mice (termed YY1<sup>iKO</sup>) to permanently disrupt YY1 function in adult Pax7<sup>+</sup> SCs upon the administration of TM. Pax7<sup>CreERT2/+</sup>;YY1<sup>+/+</sup> mice treated with TM were used as control (Ctrl). Following the administration of five consecutive doses of TM (Fig 2A), SCs were FACS-isolated and cultured; YY1 mRNA was efficiently depleted (94%, Figs 2B and EV2A). Consistently, DNA analysis also showed lack of YY1 gene in the YY1<sup>iKO</sup> genome (Fig EV2B). IF staining for YY1 protein also revealed it was eliminated from freshly isolated Pax7<sup>+</sup> SCs (FISCs) whereas readily detected in the Ctrl (Fig 2C). Furthermore, when examining freshly isolated extensor digitorum longus (EDL) myofibers from Ctrl or YY1<sup>iKO</sup> mice, loss of YY1 in SCs was also readily seen with an ablation efficacy of 94% (Figs 2D and EV2C). Lastly, on muscle cryosections YY1 protein was not detected in the majority of Pax7-expressing QSCs from YY1<sup>iKO</sup> mice, where only 6% SCs escaped recombination and remained YY1<sup>+</sup> (Fig 2E). Importantly, TM-treated YY1<sup>iKO</sup> mice remained viable and displayed no obvious phenotype or changes in body weight under physiological conditions up to 1 year after TM injection. In addition, 3 weeks after TM injection, we found no obvious change in the number of SCs isolated by FACS between Ctrl and YY1<sup>iKO</sup> littermates (Fig 2F). Consistently, the number of SCs on single myofibers did not differ between the littermates 3 days or 2 months after the TM treatment (Fig EV2D and E), indicating YY1 loss did not have impact on SC maintenance.

Next, to study the role for YY1 in muscle regeneration, we employed a commonly used cardiotoxin (CTX)-induced muscle injury-regeneration model (Chen *et al*, 2017). Tibialis anterior (TA) muscles of Ctrl or YY1<sup>iKO</sup> animals were subjected to a single CTX injury and then allowed to recover for 3–60 days before analysis of the regenerated tissue (Fig 2G). YY1<sup>iKO</sup> mice exhibited

**Figure 1. Conditional deletion of YY1 in muscle progenitor cells causes defect in cell expansion.**

- A Breeding scheme for generating conditional knock out (YY1<sup>CKO</sup>), Pax7<sup>Cre/+</sup>; YY1<sup>f/f</sup>, and control (Ctrl), Pax7<sup>+/+</sup>; YY1<sup>f/f</sup> littermates.
- B, C Immunofluorescent (IF) staining of Pax7 and YY1 was performed on cryosections of myotome or limb bud from Ctrl or YY1<sup>CKO</sup> mice to confirm the ablation of YY1 in Pax7-expressing progenitors. Scale bar = 100 μm.
- D Representative images of Ctrl, heterozygous (Het), and YY1<sup>CKO</sup> newborn (P0) mice or embryos at E18.5 day.
- E Excised lungs from P0 Ctrl or YY1<sup>CKO</sup> pups were placed in a beaker for sinking test. The lung from YY1<sup>CKO</sup> pup sank whereas Ctrl floated.
- F P0 lungs were stained with hematoxylin and eosin (H&E), and representative images are shown. Scale bar = 100 μm.
- G Representative images of diaphragms (Dps) isolated from P0 Ctrl or YY1<sup>CKO</sup> littermates.
- H The above Dps were used for H&E or immunohistochemistry (IHC) staining for MyHC. Representative images from three pairs of littermates are shown. Scale bar = 100 μm.
- I, J The above harvested Dps were subjected to IF staining for MyHC or troponin T (TnT) together with laminin. Scale bar = 50 μm. Quantifications of positively stained fibers per area are shown on the right (*n* = 3 mice, each).
- K Representative images of H&E staining of hindlimb muscles isolated from Ctrl or YY1<sup>CKO</sup> embryos at E18.5 day. Scale bar = 400 μm (left) or 50 μm (right).
- L, M The above harvested limb muscles were subjected to IF staining for MyHC or TnT together with laminin. Scale bar = 400 μm (left) or 50 μm (right). Quantifications of the numbers of MyHC<sup>+</sup> or TnT<sup>+</sup> fibers per area are shown on the right (*n* = 3 mice, each).
- N, O The above harvested limb (N) or diaphragm (O) muscles were subjected to IF staining for Pax7 and laminin. Scale bar = 100 μm (N) or 50 μm (O). Quantification of the numbers of Pax7<sup>+</sup> muscle progenitor cells per area is shown on the right (*n* = 3 mice, each).

Data information: Error bars represent SD's of the mean. Student's *t*-test (two-sided): \**P* < 0.05, \*\**P* < 0.01, \*\*\**P* < 0.001.

Source data are available online for this figure.

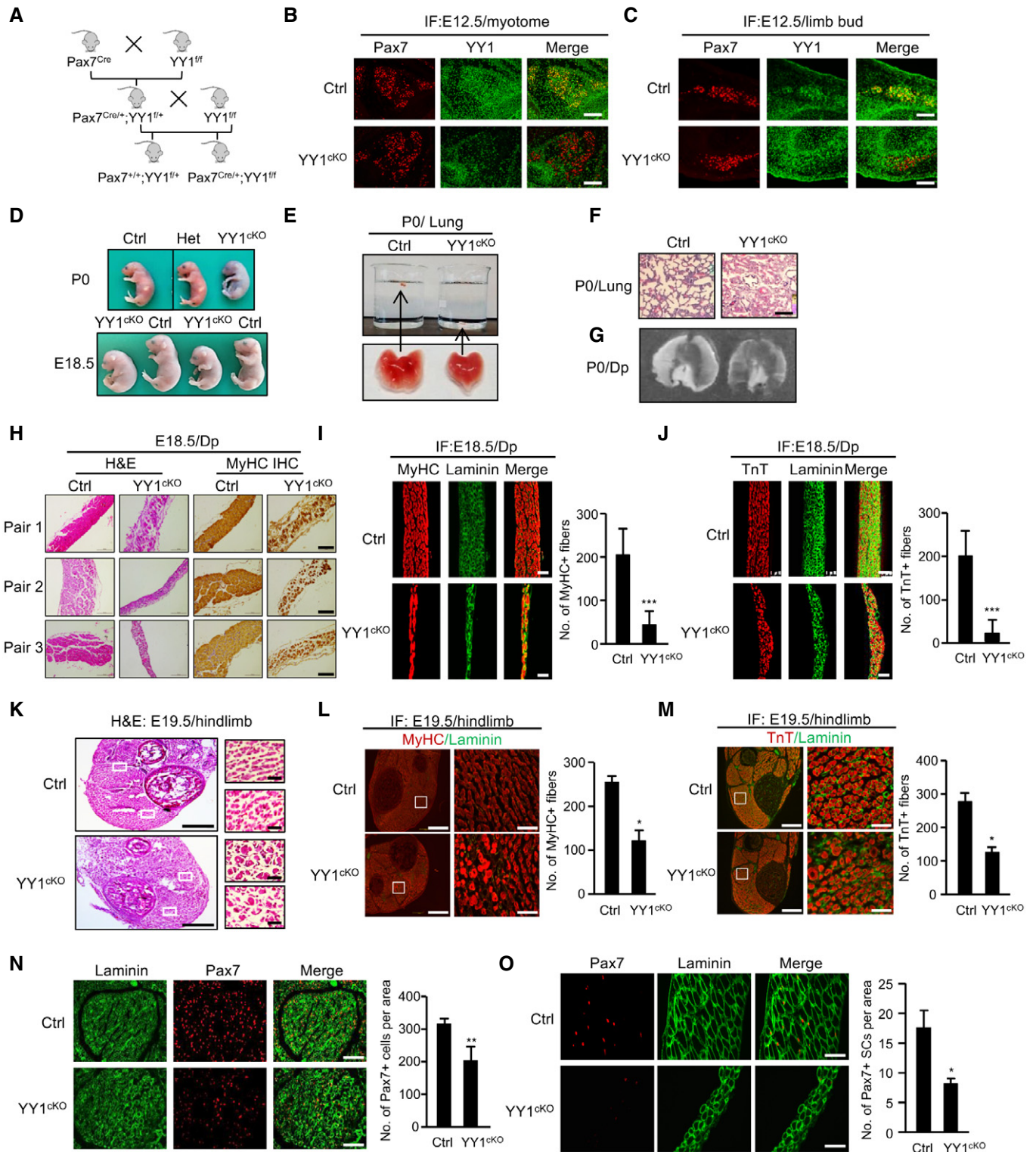


Figure 1.

normal muscle size and morphology in the absence of injury (Fig 2G, day 0). The CTX injection quickly induced extensive muscle damage and infiltration of inflammatory cells in both Ctrl and YY1<sup>iKO</sup> muscles (Fig 2G). Strikingly, muscle regeneration was severely disrupted in YY1<sup>iKO</sup> mice. In Ctrl muscle, during the acute phase of

regeneration (1–7 days after injury), SC descendants fused to form small new myofibers expressing embryonic myosin heavy chain (eMyHC) characterized by centrally localized nuclei; these eMyHC fibers were readily seen at day 5 (Fig 2H). In contrast, YY1<sup>iKO</sup> muscle was composed of degenerating myofibers, fibrotic tissues, and

inflammatory cells at this phase; eMyHC<sup>+</sup> regenerating fibers were rarely seen until day 7 when the Ctrl muscle was composed of regenerated myofibers with larger size that had down-regulated eMyHC (Fig EV2F). Fourteen days after injury, muscle damage and inflammatory cells in Ctrl muscle were largely cleared, and the regenerated myofibers continued to grow and mature, as their sizes became homogenous (Fig 2G). In contrast, YY1<sup>iKO</sup> muscle was still occupied by damaged fibers and inflammatory cells, with only traces of regenerating myofibers (Fig 2G). If left to 60 days after injury, Ctrl muscle had fully regenerated, and muscle architecture was largely restored, with the normal myofiber hypertrophy seen after injury (Fig 2I). In contrast, YY1<sup>iKO</sup> muscle nearly failed to regenerate and reconstitute muscle structure, instead it displayed severe atrophy with markedly reduced fiber size (Fig 2I and J) and evident fibrosis (Fig 2I). Collectively, these results suggested that YY1 deletion leads to severe loss of regenerative capacity, and thus, the expression of YY1 in SCs is essential for timely and proper repair of damaged skeletal muscle tissue after acute injury.

Muscle regeneration requires activation and proliferation of satellite cells and subsequent differentiation of myoblasts into myotubes. Considering embryonic deletion of YY1 caused a defect in the expansion of muscle progenitors (Fig 1N and O), we asked whether the expansion of SC pool in YY1<sup>iKO</sup> mice had been compromised. Indeed, 3 days after CTX injection, the number of SCs sorted by FACS from YY1<sup>iKO</sup> vs. Ctrl was largely reduced (66%; Fig 2K); consistently, staining of the above injured muscles for Pax7 or MyoD also revealed a significant reduction in Pax7<sup>+</sup> or MyoD<sup>+</sup> cells in YY1<sup>iKO</sup> muscle (Fig 2L and M, 73 and 67%, respectively). Interestingly, staining of Pax7 4 weeks after CTX injury revealed no difference in the number of Pax7<sup>+</sup> cells per 100 fibers between Ctrl and YY1<sup>iKO</sup> mice (Fig 2N), suggesting YY1 loss may not impact the

ability of SC to self-renew and return to quiescent stage. Consistently, no significant change was found on the number of asymmetrically dividing Pax7<sup>+</sup>MyoD<sup>+</sup> cells when monitoring the planar and apico-basal cell divisions and recording daughter cells in doublets that were identical (symmetric) or non-identical (asymmetric cell division; Fig EV2G). Nevertheless, when the mice were subject to the second CTX injury 28 days after the first injury (Fig 2O), compared to the first injury, YY1<sup>iKO</sup> mice suffered from an even more severely hampered regeneration (Fig 2P–S, 88% reduction in eMyHC<sup>+</sup> fibers in iKO vs. Ctrl) and nearly complete loss of SC expansion (Fig 2T, 91% loss of Pax7<sup>+</sup> cells in iKO vs. Ctrl). Altogether, the above results confirmed the key role of YY1 in SC expansion during acute injury-induced muscle regeneration.

### YY1 deletion aggravates dystrophic phenotype in mdx mice

To further solidify the impact of YY1 deletion on injury-induced muscle regeneration, we next employed a mdx mouse, in which mutation in dystrophin gene leads to continuous degeneration and regeneration of myofibers accompanied by repeated activation and enhanced turnover of SCs, mimicking the phenotype of human DMD (Bulfield *et al*, 1984). YY1<sup>iKO</sup> mice were crossed with mdx mice to generate double KO (dKO) mice. Two-month-old Pax7<sup>CreERT2/+</sup>; YY1<sup>f/f</sup>; mdx mice were treated with five consecutive doses of TM to delete YY1 in SCs; Pax7<sup>CreERT2/+</sup>; YY1<sup>+/+</sup>; mdx mice treated with TM were used as control (Ctrl; Fig 3A and B). After 4 months, YY1<sup>dKO</sup> had a much smaller body size than Ctrl littermates (Fig 3C). The size and weight of limb muscles including TA, gastrocnemius (GAS), and quadruple (Quad) were all markedly reduced (50, 53, and 45%; Fig 3D and E). Likewise, Dp muscle was markedly thinner (Fig 3F). Further histological examination revealed a reduced

#### Figure 2. Inducible ablation of YY1 in adult mouse muscle blocks injury-induced muscle regeneration.

- A Schematic outline of the tamoxifen (TM) administration used in the study and experimental design for testing the effect of YY1 deletion on cardiotoxin (CTX)-induced muscle regeneration process for control (Ctrl), Pax7<sup>CreERT2/+</sup>; YY1<sup>+/+</sup> and inducible knock out (YY1<sup>iKO</sup>), Pax7<sup>CreERT2/+</sup>; YY1<sup>f/f</sup> mice.
- B SCs were FACS-sorted 3 days after the last TM injection and cultured for 1.5 days; RT-qPCR detection of YY1 mRNA shows the ablation in YY1<sup>iKO</sup> cells.
- C–E IF staining for Pax7 and YY1 on (C) freshly isolated FISCs or (D) single myofibers from EDL muscles or (E) cryosections from TA muscles showing the deletion of YY1 protein from YY1<sup>iKO</sup> cells. Scale bar = 100  $\mu$ m in (C) or 50  $\mu$ m in (D, E).
- F Representative FACS plots. About 100,000 cells from 2-month-old Ctrl and YY1<sup>iKO</sup> mice were sorted by FACS 3 weeks post-TM injection. The percentage of SCs was shown. (*n* = 3 mice, each).
- G H&E staining was performed on the injured TA muscles collected from the designated times post-CTX injection to visualize the degree of regeneration. Scale bar = 100  $\mu$ m.
- H IF staining for eMyHC on the TA muscles 5 days post-CTX injury. Quantifications of the number of eMyHC<sup>+</sup> fibers are shown on the right (*n* = 3, each). Scale bar = 50  $\mu$ m.
- I Left: representative images of TA muscles isolated from Ctrl or YY1<sup>iKO</sup> mice 60 days post-CTX injury. Right: Masson's trichrome staining of the above muscles to visualize the degree of fibrosis. Scale bar = 100  $\mu$ m.
- J Cross-section area (CSA) of individual myofibers in TA muscles 4 weeks after injury was measured. The distribution for CSA was calculated (*n* = 3 mice).
- K Representative FACS plots showing the percentage of SCs sorted from TA muscles 3 days after CTX injury of Ctrl and YY1<sup>iKO</sup> mice.
- L, M Immunostaining for Pax7 or MyoD together with laminin was performed on the TA muscles 3 days post-CTX injury. Scale bar = 100  $\mu$ m. Quantifications of the numbers of Pax7<sup>+</sup> or MyoD<sup>+</sup> SCs per area are shown on the right (*n* = 3 mice, each).
- N IF staining for Pax7 and laminin on TA muscles 4 weeks after CTX injury of Ctrl or YY1<sup>iKO</sup> mice. Quantifications of the numbers of Pax7<sup>+</sup> SCs per 100 fibers are shown on the right (*n* = 3 mice, each). Scale bar = 100  $\mu$ m.
- O Schematic outline of the second CTX injury 28 days after the first injury.
- P H&E staining was performed on TA muscles of Ctrl or YY1<sup>iKO</sup> mice 7 days after second CTX injury. Scale bar = 400  $\mu$ m (left) or 100  $\mu$ m (right).
- Q Representative images of above TA muscles 7 days after second injury.
- R Quantifications of the weight of above TA muscles from three pairs of littermate mice.
- S IF staining for eMyHC and laminin on TA muscles 7 days after the second CTX injury of Ctrl or YY1<sup>iKO</sup> mice. Quantifications of the number of eMyHC<sup>+</sup> fibers per area are shown on the right (*n* = 3 mice, each). Scale bar = 100  $\mu$ m.
- T IF staining for Pax7 and laminin on the above muscles and the quantifications of the number of Pax7<sup>+</sup> SCs per area are shown on the right (*n* = 3 mice, each). Scale bar = 100  $\mu$ m.

Data information: Error bars represent SD's of the mean. Student's *t*-test (two-sided): N.S = non-significant, \**P* < 0.05, \*\**P* < 0.01, \*\*\**P* < 0.001. Source data are available online for this figure.

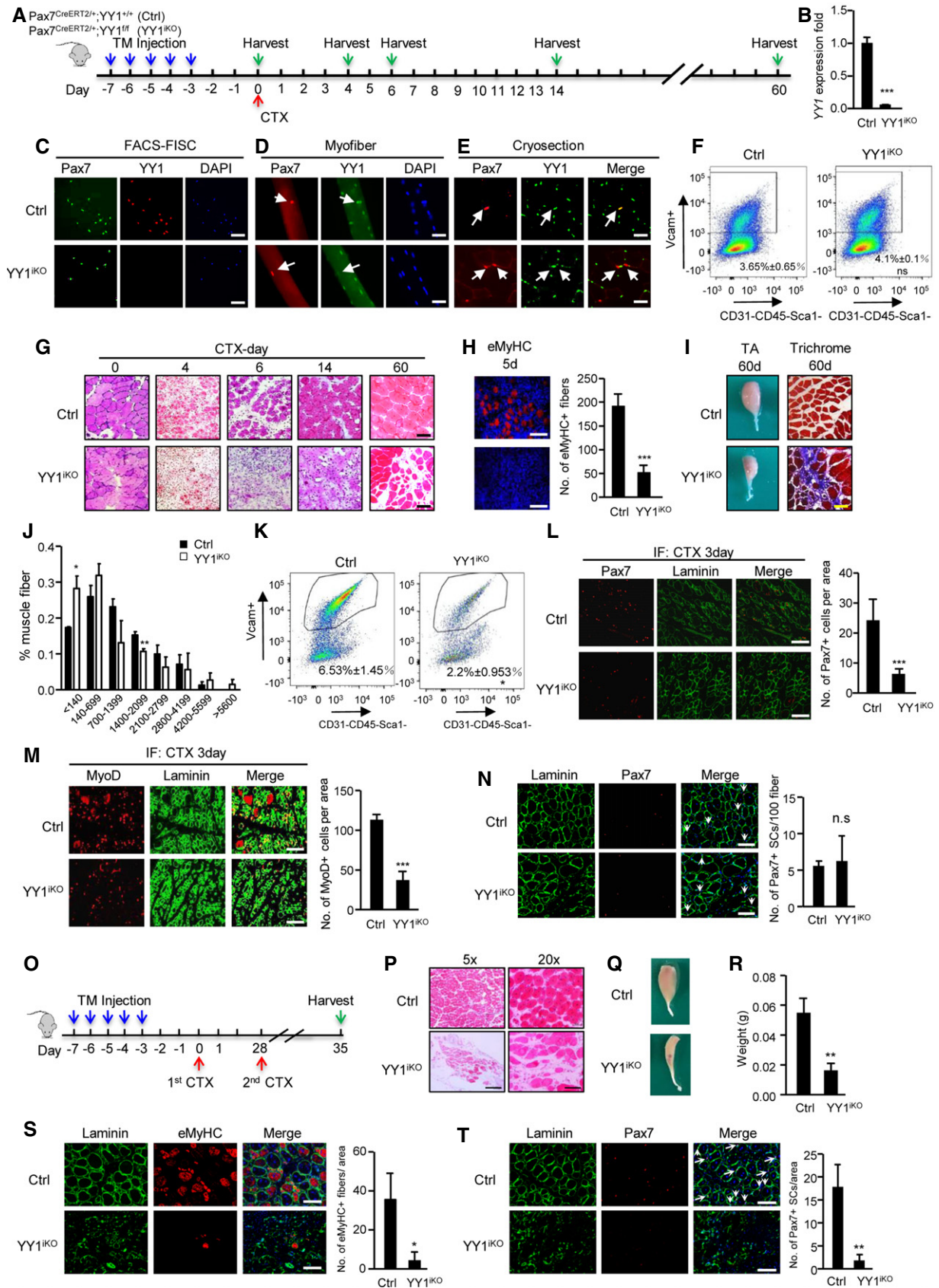


Figure 2.

number of muscle fibers (Fig 3G and H, MyHC staining) accompanied by an exacerbation of fibrosis (Fig 3I and J, collagen and trichrome staining) in both limb (TA) and Dp muscles. Moreover, a higher number of hypertrophic myofibers was found in YY1<sup>dko</sup> vs. Ctrl mice (Fig 3K). Altogether, the above findings suggested that the deletion of YY1 in SCs of mdx aggravates dystrophic phenotypes. Expectedly, a largely reduced number of SCs (70%) was sorted out by FACS from TA muscles of YY1<sup>dko</sup> vs. Ctrl mice (Fig 3L); consistently, the number of Pax7<sup>+</sup> cells was also largely reduced by 71% (Fig 3M), suggesting YY1 deletion led to a defect in SC expansion during the regeneration in a chronic muscle injury setting. Lastly, to confirm the functional consequence of the weakened muscles in YY1<sup>dko</sup>, the mice were subjected to muscle functional test by detecting the maximal isometric tetanic force on EDL and soleus (SOL) muscles. As expected, the muscles from YY1<sup>dko</sup> showed impaired tetanus force (Fig 3N and O, reduced by 43 and 54%, respectively) compared to the Ctrl. Altogether, the above findings led us to conclude that YY1 plays an essential role in maintaining SC pool and enables continuous muscle regeneration under chronic injury.

### YY1 deletion leads to cell-autonomous defect in SC activation and proliferation

To further investigate the cellular mechanism underlying the hampered SC pool expansion in YY1<sup>dko</sup> mice, we first examined YY1 expression dynamics in SCs and found it was lowly expressed in FISCs but quickly induced upon SC activation and its level continued to increase into 48 h as SCs fully activated and proliferated (Figs 4A and B, and EV3A); this pattern was concomitant with a sharp increase in YY1 mRNA level in the acute SC activation/proliferation phase after CTX injection (Fig EV3B). The above data led us to speculate that YY1 may promote the proliferative expansion of SCs. To test this notion, freshly isolated SCs (FISCs) by FACS sorting were cultured and labeled by 5-ethynyl-2'-deoxyuridine (EdU; Fig EV3C). YY1-depleted SCs showed a marked reduction in the number of EdU<sup>+</sup> cells at 48 h in culture (Figs 4C, and EV3D and E), reflecting a proliferative delay; this was also confirmed by a marked reduction in the number of Pax7<sup>+</sup>MyoD<sup>+</sup> cells (Figs 4D and EV3F). Furthermore, when freshly isolated EDL myofiber explants were cultured for 2 days to allow SC activation and proliferation on the

fibers, the number of Pax7<sup>+</sup>MyoD<sup>+</sup> cells from YY1<sup>dko</sup> myofibers was also significantly reduced compared with the Ctrl (Fig 4E, 42%). The proportion of Pax7<sup>+</sup>MyoD<sup>+</sup> cells (Fig EV3G), on the other hand, showed no significant difference, suggesting that although the cell proliferation was delayed the lineage progression was not blocked. Consistently, when stained for Ki67 and Pax7, a much lower number of double positive cells was found on the YY1<sup>dko</sup> myofibers (Fig 4F, 56.24%). When further examined *in vivo* (Fig EV3H), EdU labeling in regenerating muscles for 12 h also revealed a reduced (12%) number of proliferating SCs at 2.5 days after CTX injury (Fig 4G). Altogether, the above results solidified the delayed proliferation caused by YY1 loss. To pinpoint the possible defect in the earlier stage, i.e., activation of quiescent SCs to enter the first cell division, we found that at 24 h before SCs entered the first cell cycle (Tang & Rando, 2014), the number of EdU<sup>+</sup> cells was reduced (10%) in YY1<sup>dko</sup> SCs (Fig 4H), indicating a possible defect at the very early activation stage. To solidify the notion, we found the percentage of MyoD<sup>+</sup> cells was significantly decreased when examining the single myofibers cultured in growth medium for 12 or 24 h (Fig 4I and J) but not 48 h (Fig EV3I). Lastly, lentiviral re-expression of YY1 in YY1<sup>dko</sup> cells (Fig EV3J) indeed restored the proliferative capacity of these cells (Fig 4K), pinpointing YY1 loss as the cause of the defect. Interestingly, YY1<sup>dko</sup> SCs did not show an increased propensity for differentiation as seen in other cases (Zhu *et al*, 2016); the number of Myog<sup>+</sup>MyoD<sup>+</sup> cells on YY1<sup>dko</sup> myofibers at day 3 in culture was instead largely reduced (97% of Ctrl level, Fig 4L). In addition, SCs from YY1<sup>dko</sup> mice did not form MyHC<sup>+</sup> myotubes efficiently when differentiated (50% of Ctrl level, Fig 4M). Furthermore, TUNNEL assay revealed no evident apoptosis (Fig EV3K). Altogether, the above results demonstrated that inducible YY1 deletion in Pax7-expressing SCs causes cell-autonomous defect in their activation and proliferation capacity.

### Transcriptomic and global binding profiling reveals YY1 repression of mitochondrial genes in SCs

To probe into the molecular mechanisms underlying YY1 influence on SCs activation/proliferation, we performed RNA sequencing (RNAseq) to interrogate the transcriptomic changes caused by YY1 loss. Total RNAs from ASCs (cultured for 36 h) were extracted and

**Figure 3. YY1 deletion aggravates dystrophic phenotype in mdx mice.**

- A Outline of the TM administration scheme to obtain Ctrl or YY1<sup>dko</sup> mice.
- B SCs were FACS-sorted 4 months after the last TM injection; RT-qPCR detection of YY1 mRNA shows the ablation in YY1<sup>dko</sup> cells.
- C Representative images of Ctrl or YY1<sup>dko</sup> mice 4 months after the TM administration.
- D Representative images of limb muscles (tibialis anterior, TA; gastrocnemius, Gas; quadruple, Quad) from Ctrl or YY1<sup>dko</sup> mice.
- E Quantifications of muscle weight from three pairs of littermate mice.
- F Representative images of Dp muscles isolated from Ctrl or YY1<sup>dko</sup> mice 4 months after the TM injection.
- G, H (G) H&E or (H) MyHC staining was performed on TA or Dp muscles from Ctrl or YY1<sup>dko</sup> mice. Quantifications of the numbers of MyHC<sup>+</sup> fibers per area of TA or Dp muscles are shown on the right (*n* = 3 mice, each). Scale bar = 100 μm.
- I, J (I) Collagen 1 or (J) Masson's trichrome staining was performed on TA or Dp muscles from Ctrl or YY1<sup>dko</sup> mice. Scale bar = 100 μm.
- K The distribution of fiber size measured by CSA in TA muscles from three pairs of 6-month-old Ctrl and YY1<sup>dko</sup> mice was calculated (*n* = 3 mice, each).
- L Representative FACS plots showing the percentage of SCs sorted from 6-month-old Ctrl and YY1<sup>dko</sup> mice (*n* = 3 mice, each).
- M IF staining for Pax7 and laminin on TA muscles of Ctrl or YY1<sup>dko</sup> mice. Quantifications of the numbers of Pax7<sup>+</sup> SCs per 100 fibers are shown on the right (*n* = 3 mice, each).
- N, O EDL or SOL muscles from Ctrl or YY1<sup>dko</sup> mice were subjected to measurement of maximal isometric tetanic force. Left: representative trace images of normalized tetanic force. (Right): quantification of the force by normalizing with cross-sectional area (CSA; *n* = 3 mice, each).

Data information: Error bars represent SD's of the mean. Student's *t*-test (two-sided): \**P* < 0.05, \*\**P* < 0.01, \*\*\**P* < 0.001.

Source data are available online for this figure.

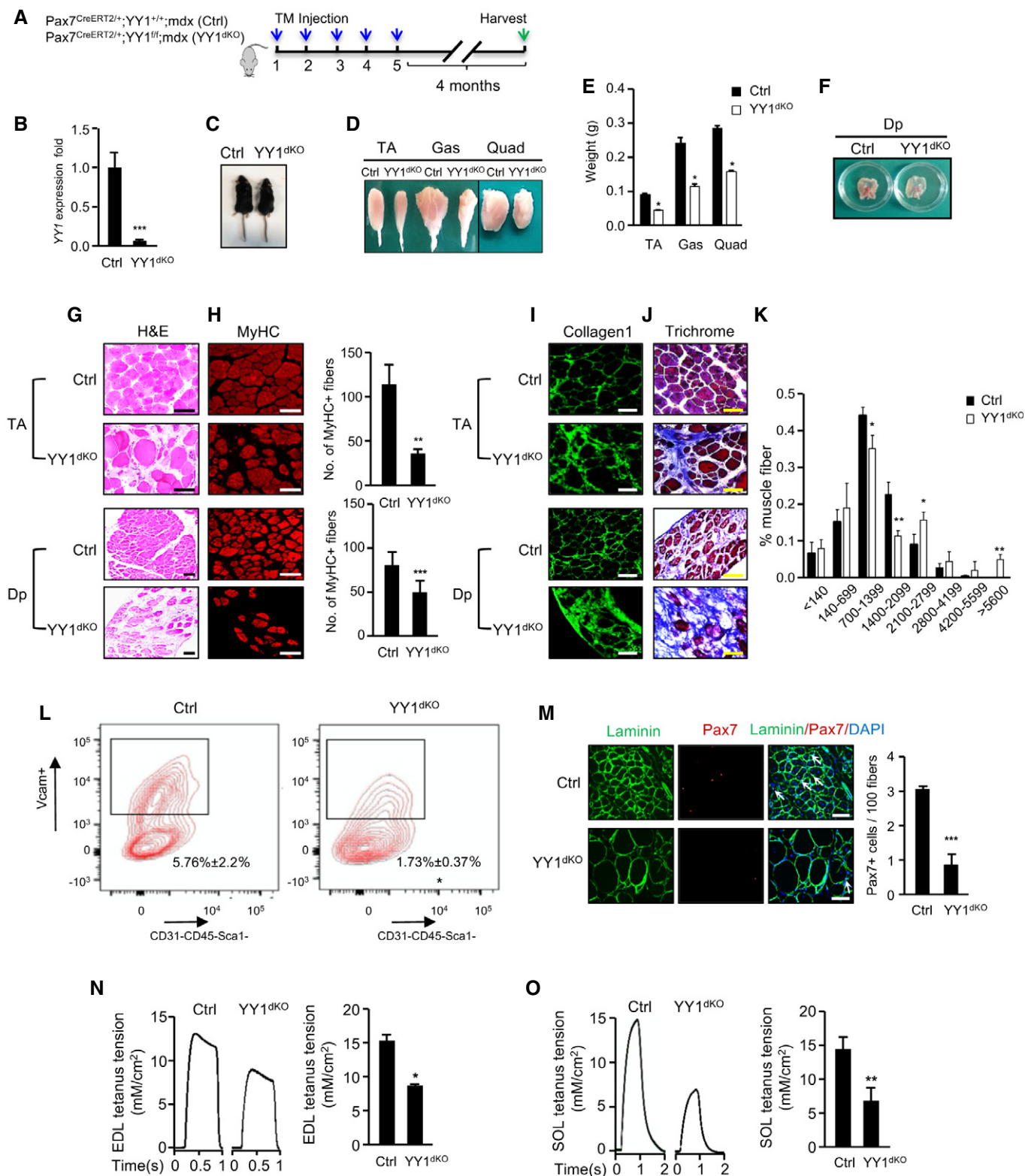


Figure 3.

subject to PolyA<sup>+</sup> RNAseq. A total of 979 genes were up-regulated whereas 924 down-regulated in YY1<sup>iKO</sup> vs. Ctrl (Fig 5A; Table EV1). Forty-nine lincRNAs were found differentially expressed, which is in

line with our prior finding that YY1 regulates dozens of lincRNAs in C2C12 myoblasts (Lu *et al*, 2013). Gene Ontology (GO) analysis revealed terms such as “cell cycle” and “cell division” are



prominent among the down-regulated transcripts (Fig EV4B; Table EV1), consistent with the observed delay in cell activation/proliferation (Fig 4). Interestingly, the up-regulated genes were dominant by mitochondrion-related GO terms such as “mitochondrial membrane”, “mitochondrial envelope”, and “mitochondria part” (Fig 5B and C; Table EV1). Gene set enrichment analysis (GSEA) also disclosed that the up-regulated genes were enriched in oxidative phosphorylation (OXPHOS) pathway (Fig 5D). Specifically, among the enriched mitochondrial genes, genes related to (i) electron transport chain, including *Ndufa2*, *Ndufb3*, *Uqcrl1*, and *Cox7a2*; (ii) mitochondrial translation, including *Mrpl11*, *Mrpl52*, *Mrpl13*, and *Chchd1*; (iii) purine nucleoside triphosphate metabolic process, including *ATP5j2*, *ATP5f1*, *ATP5o*, and *Nme1*; and (iv) mitochondrial transmembrane transporter, including *Tomm5*, *Timm9*, and *Slc25a33*, were found on the top of the list (Table EV1). Additionally, an array of genes such as *Sod1*, *Nox1*, and *Txn1*, correlated to regulate cellular redox homeostasis, were also up-regulated (Table EV1). The above RNAseq results were further confirmed by RT-qPCR on several selected genes including *Atp5l*, *Cox4i1*, *Ndufa2*, *Ndufb3*, and *Uqcrl1* (Fig 5E). Examining more closely into the expression of Complexes I–V, we found that the majority of subunits in Complexes I, III, IV, and V were up-regulated by RNAseq (Fig EV4A), which was substantiated by the elevated protein expression levels of Sdhb (Complex II subunit, 30 kDa), Uqcrc2 (Complex III subunit, 48 kDa), and Atp5a (Complex V subunit, 55 kDa) using a mitoprofile antibody cocktail for Western detection (Fig 5F). Curious about the potential expression changes in myogenic genes, by GSEA, we found that down-regulated genes were not enriched in myogenic genes, further supporting a role for YY1 in cell proliferation but not lineage progression (Fig EV4C and D). Furthermore, when total RNAs from FISCs were

subject to transcriptomic profiling (Fig 5G; Table EV2), mitochondrion-related genes were also markedly enriched in the up-regulated panel of genes (Fig 5H; Table EV2), including *Cox8b*, *Nme4*, *Slc25a29*, *Nnt1*, *Cox7a1*, *Rars2*, *Lars2*, and *Hscb* (Figs 5I, and EV4E and F), despite the down-regulated genes were enriched for “extracellular region part” etc. (Fig EV4G; Table EV2), distinct from those identified in ASCs. Together, the above findings led us to speculate that YY1 functions to repress mitochondrial genes and oxidative phosphorylation.

To further pinpoint whether YY1 represses the mitochondrial genes through direct binding and transcriptional regulation, genome-wide chromatin immunoprecipitation coupled with massive parallel sequencing (ChIPseq) was performed on chromatin from ASCs isolated from C57B/L wild-type mice, which led to the identification of a total of 2,031 binding peaks (Table EV3). Expectedly, these peaks distributing in intergenic, gene body, and promoter regions (Fig 5J) were enriched for a bona fide YY1 binding motif (Fig 5K). Gene Ontology (GO) analysis revealed terms such as “nucleoplasm” and “mitochondrial small ribosomal subunit” were prominent among genes with YY1 binding at promoters (Fig EV4H). When intersecting with the 979 genes up-regulated from RNAseq, 90 were found to be likely direct targets of YY1 with binding in promoter regions (Fig 5L), whereas the majority of genes may be indirectly activated upon YY1 deletion. Strikingly, these genes were extremely enriched for mitochondrion/OXPHOS-related terms, such as “respiratory chain”, “mitochondrial part”, and “electron transport chain”, but “cell cycle” or “cell division” related terms no longer appeared (Fig 5M; Table EV3). From both the ChIPseq (Fig 5N) and ChIP-qPCR validation (Fig 5O), these mitochondrial genes were bound by YY1 in their transcriptional start site (TSS) regions, suggesting a direct transcriptional regulation. Of note, the majority

**Figure 4. YY1 deletion leads to cell-autonomous defect in SC pool expansion.**

- A FACS-isolated SCs from Pax7-nGFP mice were cultured for the designated time (0, 24, 48, or 72 h). YY1 expression was quantified by RT-qPCR. *18S* was used as the normalization control.
- B Flow cytometric analysis of YY1 protein or IgG control in FACS-isolated SCs cultured for the designated time (0, 24, or 48 h). YY1 protein level is normalized to IgG levels. The numbers indicate the normalized level of YY1 protein relative to that of FISCs.
- C An equal number of FACS-isolated SCs from Ctrl or YY1<sup>KO</sup> mice were cultured for 48 h and EdU-labeled for 8 h, followed by immunostaining for Pax7 (green) and EdU (red). Quantifications of the percentage of EdU<sup>+</sup> cells are shown on the right ( $n = 3$  mice, each). Scale bar = 100  $\mu$ m.
- D The above cells were also IF-stained for Pax7 (red) and MyoD (green). Quantifications of each population, Pax7<sup>+</sup>MyoD<sup>+</sup> or Pax7<sup>-</sup>MyoD<sup>+</sup>, are shown on the right ( $n = 3$ , each). Scale bar = 100  $\mu$ m.
- E Single EDL myofibers were cultured for 48 h before staining for Pax7 (red) and MyoD (green). Quantifications of the numbers of each population, Pax7<sup>+</sup>MyoD<sup>-</sup>, Pax7<sup>-</sup>MyoD<sup>+</sup>, or Pax7<sup>+</sup>MyoD<sup>+</sup>, are shown on the right ( $n = 3$  mice, each). Scale bar = 50  $\mu$ m.
- F Pax7 (green) and Ki67 (red) staining was performed on the above single EDL myofibers. Scale bar = 50  $\mu$ m. Quantifications of the numbers of each population, Pax7<sup>+</sup>Ki67<sup>-</sup>, Pax7<sup>-</sup>Ki67<sup>+</sup>, or Pax7<sup>+</sup>Ki67<sup>+</sup>, are shown on the right ( $n = 3$  mice, each).
- G SCs expansion *in vivo* was determined by EdU labeling for 12 h 2.5 days after CTX injury. Quantifications of the numbers of EdU<sup>+</sup> cells are shown on the right ( $n = 3$  mice, each). Scale bar = 100  $\mu$ m.
- H An equal number of FACS-isolated SCs from Ctrl or YY1<sup>KO</sup> mice were cultured for 24 h and EdU-labeled for 12 h, followed by immunostaining for Pax7 (green) and EdU (red) was performed. Quantifications of the percentage of EdU<sup>+</sup> cells are shown on the right ( $n = 3$  mice, each). Scale bar = 100  $\mu$ m.
- I, J Single EDL myofibers were cultured for 12 (I) or 24 (J) h in growth media before staining for Pax7 (green) and MyoD (red). Scale bar = 50  $\mu$ m. Quantifications of the proportion of MyoD<sup>+</sup> cells are shown on the right ( $n = 3$  mice, each).
- K FACS-isolated SCs from YY1<sup>KO</sup> mice were infected with YY1-expressing or control viruses, followed by immunostaining for Pax7 (green) and MyoD (red) 36 h post-transfection. Scale bar = 100  $\mu$ m. Quantifications of the numbers of each population, Pax7<sup>+</sup>MyoD<sup>-</sup>, Pax7<sup>-</sup>MyoD<sup>+</sup>, or Pax7<sup>+</sup>MyoD<sup>+</sup>, are shown on the right ( $n = 3$  mice, each).
- L Single EDL myofibers were cultured for 3 days, followed by immunostaining for myogenin (red) and MyoD (green). Scale bar = 50  $\mu$ m. Quantifications of the numbers of each population, MyoD<sup>+</sup>Myog<sup>+</sup>, MyoD<sup>-</sup>Myog<sup>+</sup>, or MyoD<sup>+</sup>Myog<sup>-</sup>, are shown on the right ( $n = 3$  mice, each).
- M FACS-isolated SCs were cultured for 2 days in proliferation medium followed by 2 days in differentiation medium; the degree of differentiation was assessed by IF staining of MF20<sup>+</sup>. Scale bar = 100  $\mu$ m. Quantifications of the numbers of MF20<sup>+</sup> area per nucleus are shown on the right ( $n = 3$  mice, each).

Data information: Error bars represent SD's of the mean. Student's *t*-test (two-sided): \* $P < 0.05$ , \*\* $P < 0.01$ , \*\*\* $P < 0.001$ .

Source data are available online for this figure.

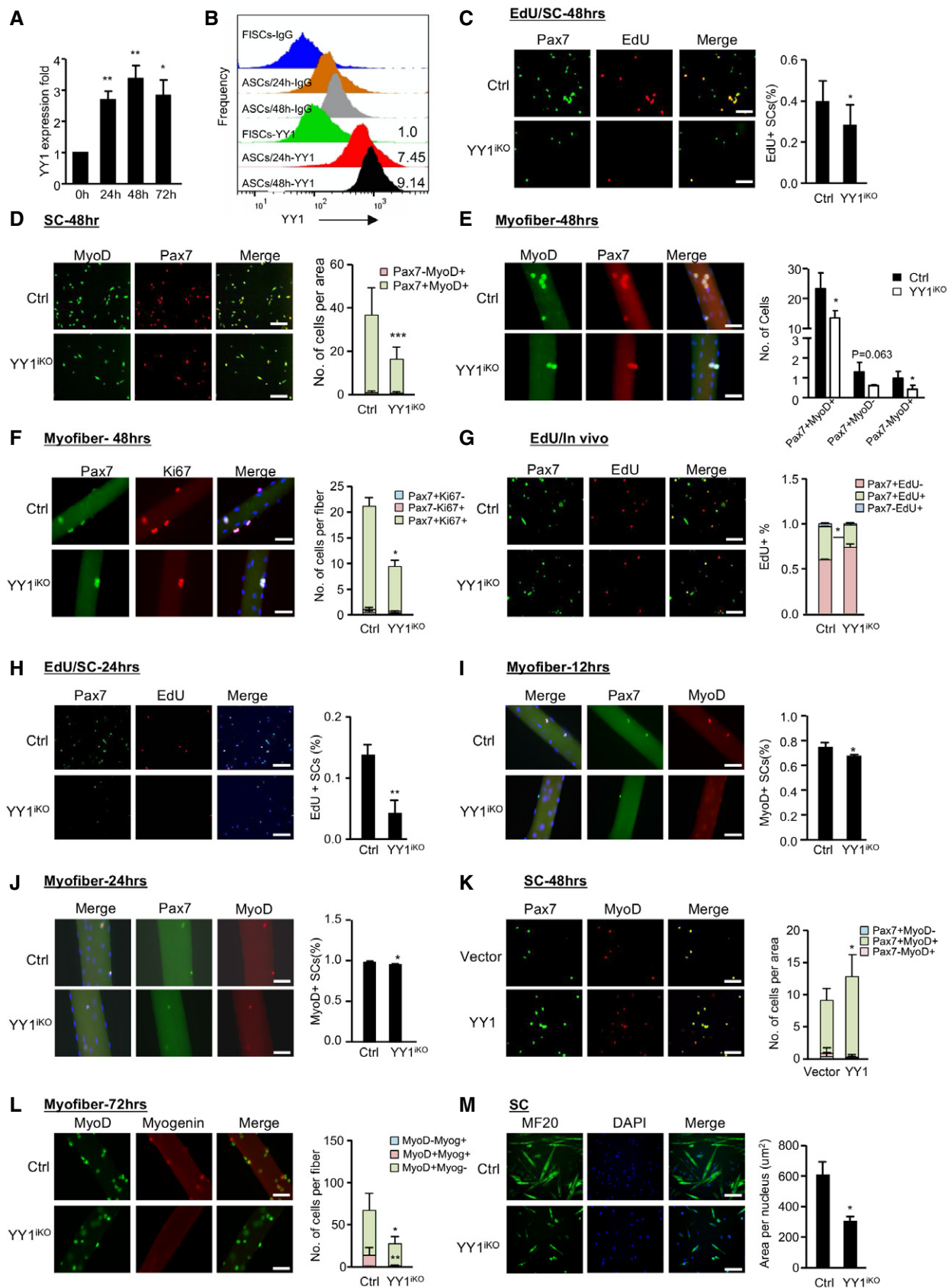


Figure 4.

of the above YY1 ChIPseq peaks in ASCs did not overlap with those previously identified in C2C12 myoblasts (Fig EV4I), reflecting the intrinsic difference between the isolated satellite cells and the myoblast cell line. Nevertheless, the 466 peaks shared between the ASC and C2C12 datasets were associated with genes enriched high in “mitochondrion part” “mitochondria” (Fig EV4J), again pointing to YY1 as a key regulator of mitochondria function in myoblast cells. Altogether, our findings suggested that YY1 acts to bind and repress mitochondrial genes upon SC activation. Since it is known that polycomb repressive complex 2 (PRC2) can interact with YY1 to deposit H3K27me3 marks and repress multiple myogenic loci in myoblasts (Carette *et al*, 2004; Wang *et al*, 2008), we asked whether this synergism also occurs to repress mitochondrial loci in SCs. Indeed, examining available Ezh2 ChIPseq data (Mousavi *et al*, 2012), we found that co-binding of Ezh2 with YY1 is evident on a list of mitochondrial genes that were up-regulated in YY1<sup>iKO</sup> cells (Fig EV4K). Further validation by ChIP–PCR using antibodies against Ezh2 or Suz12 confirmed the PRC2 binding on several mitochondrial genes (Fig 5P and Q) as well as the enrichment of H3K27me3 on the same loci (Fig 5R). In line with this, Ezh2 loss in mouse was shown to cause a defect in SC proliferation and muscle regeneration (Juan *et al*, 2011), phenocopying YY1<sup>iKO</sup>. Moreover, in order to substantiate that YY1 represses mitochondrial genes through its direct DNA-binding activity, re-expression of a wild-type (WT) YY1 restored the elevated mitochondrial genes in iKO SCs, but a mutant YY1 (S365D) lacking DNA-binding activity failed to do so (Alexander & Rizkallah, 2017); similarly, a second mutant, YY1 (1–394), lacking DNA-binding domain also did not restore the mitochondrial expression in iKO SCs (Figs 5S and EV4L). Lastly, as YY1/PRC2 was previously reported to repress Pax7 expression, upon p38 activation (Palacios *et al*, 2010), we tested whether Pax7 expression is increased by YY1 loss and surprisingly found Pax7 was decreased in iKO vs. Ctrl SCs (Fig EV4M); this is

probably because the YY1/PRC2 repression on Pax7 occurs upon myoblast fusion to myotube but not in actively proliferating myoblast cells (Palacios *et al*, 2010). In addition, treatment of ASCs with SB202190 (SB), a p38 inhibitor, led to up-regulation of mitochondrial genes in Ctrl but not YY1<sup>iKO</sup> cells; overexpressing YY1 restored mitochondrial gene expression in iKO when the cells were treated with SB, altogether suggesting that YY1/PRC2-mediated repression of mitochondrial genes is p38-dependent (Fig EV4N–P).

#### YY1 loss leads to a defect in activating glycolytic pathway during SC activation via decreasing Hif1 $\alpha$ protein

Altogether, the above genome-wide interrogation revealed a key role of YY1 in repressing mitochondrial genes in ASCs, leading us to speculate that mitochondrial function needs to be inhibited during SCs activation and proliferation. Indeed, a role for the metabolic switch from fatty acid oxidation to aerobic glycolysis is thought to occur to support increased macromolecule biosynthesis during SC activation (Ryall *et al*, 2015). In line with this notion, we found that treatment of ASCs with a glycolytic inhibitor 2-Deoxy-D-glucose (2-DG) drastically reduced ATP production even at 1 mM concentration, whereas treatment with a respiration inhibitor sodium azide (NaN<sub>3</sub>) caused a decrease of ATP production at 1 mM but the level bounced back at higher concentrations (10 and 20 mM; Fig 6A). Consistently, 2-DG treatment markedly inhibited SC proliferation (98% reduction) while NaN<sub>3</sub> caused much milder effect (62% reduction) compared to PBS-treated cells by MTS assay (Fig 6B); EdU labeling assay also confirmed the above result showing a 81% reduction in EdU<sup>+</sup> SCs upon 2-DG treatment (Fig 6C). The above hypersensitivity to the cytotoxicity of 2-DG indicated ASCs are indeed more dependent on glycolysis than OXPHOS. We thus suspected that in addition to the elevated mitochondrial genes, the YY1<sup>iKO</sup> cells might also suffer from hindered activation of glycolytic

#### Figure 5. Transcriptomic and binding profiling reveals YY1 repression of mitochondrial genes in SCs.

- A RNAseq was performed with RNAs extracted from ASCs (FACS purified and cultured for 36 h) of YY1<sup>iKO</sup> or Ctrl mice; scatter plot shows differentially expressed genes with a fold change  $\geq 2$  (red dots) in YY1<sup>iKO</sup> vs. Ctrl.
- B Gene ontology (GO) analyses of the above up-regulated genes. The top 10 enriched GO terms are displayed on the Y axis and adjusted P values on the X axis.
- C Genomic snapshots showing the examples of mitochondrial genes (*Uqcrl1*, *Mrp11*, *Apo5a*, and *Nme4*) up-regulated in YY1<sup>iKO</sup> vs. Ctrl cells.
- D GSEA analysis shows oxidative phosphorylation gene set is enriched in YY1<sup>iKO</sup> vs. Ctrl cells ( $P$ -value < 0.0001).
- E RT–qPCR validation of the expression of the selected up-regulated mitochondrial genes in YY1<sup>iKO</sup> vs. Ctrl.
- F Protein levels of the respiratory chain complexes I–V components in YY1<sup>iKO</sup> vs. Ctrl ASCs were detected using a mitoprofile antibody cocktail.  $\beta$ -actin was used as the loading control.
- G RNAseq was performed using RNAs from freshly isolated SCs (FISCs); scatter plot shows differentially expressed genes with a fold change  $\geq 2$  (red dots) in YY1<sup>iKO</sup> vs. Ctrl.
- H GO analysis for the up-regulated genes in YY1<sup>iKO</sup> vs. Ctrl.
- I Genomic snapshots show the selected mitochondrial genes (*Cox8b*, *Nme4*, *Slc25a29*, *Nnt*) up-regulated in YY1<sup>iKO</sup> vs. Ctrl FISCs.
- J ChIPseq was performed using chromatin from WT ASCs, and the genomic distribution of 2,031 YY1 binding peaks is shown.
- K *De novo* motif prediction by DREME revealed the enrichment of canonical YY1 motifs in the above binding regions.
- L Venn diagrams show the overlapping (90 genes) between the above identified binding target genes (1,387) and the up-regulated genes from ASC RNAseq (979).
- M GO analysis of the above 90 genes revealed an extreme enrichment of mitochondrial-related terms.
- N Genomic snapshots of two of the above identified mitochondrial genes (*Tomm40l* and *Ndufa13*) that are bound by YY1 in their TSSs (ChIPseq tracks) and up-regulated by YY1 deletion (RNAseq tracks).
- O ChIP–qPCR validation of YY1 binding on some mitochondrial genes. Negative control (NC) represents a genomic region on Chromosome 11 with no YY1 binding peak identified. Enrichment fold was calculated as the amount of amplified DNA from YY1 binding sites normalized to values obtained from IgG control.
- P–R ChIP–qPCR was performed to show the enrichment of Ezh2 (P), Suz12 (Q), and H3K27 me3 (R) binding on selected mitochondrial genes.
- S A construct to express wild-type YY1(WT) or two mutants lacking DNA-binding activity, YY1(1–394) and YY1(S365D), were transfected into YY1<sup>iKO</sup> cells; the expression of mitochondrial gene was measured.

Data information: Error bars represent SD's of the mean. Student's *t*-test (two-sided): N.S = non-significant, \* $P$  < 0.05, \*\* $P$  < 0.01, \*\*\* $P$  < 0.001. Source data are available online for this figure.

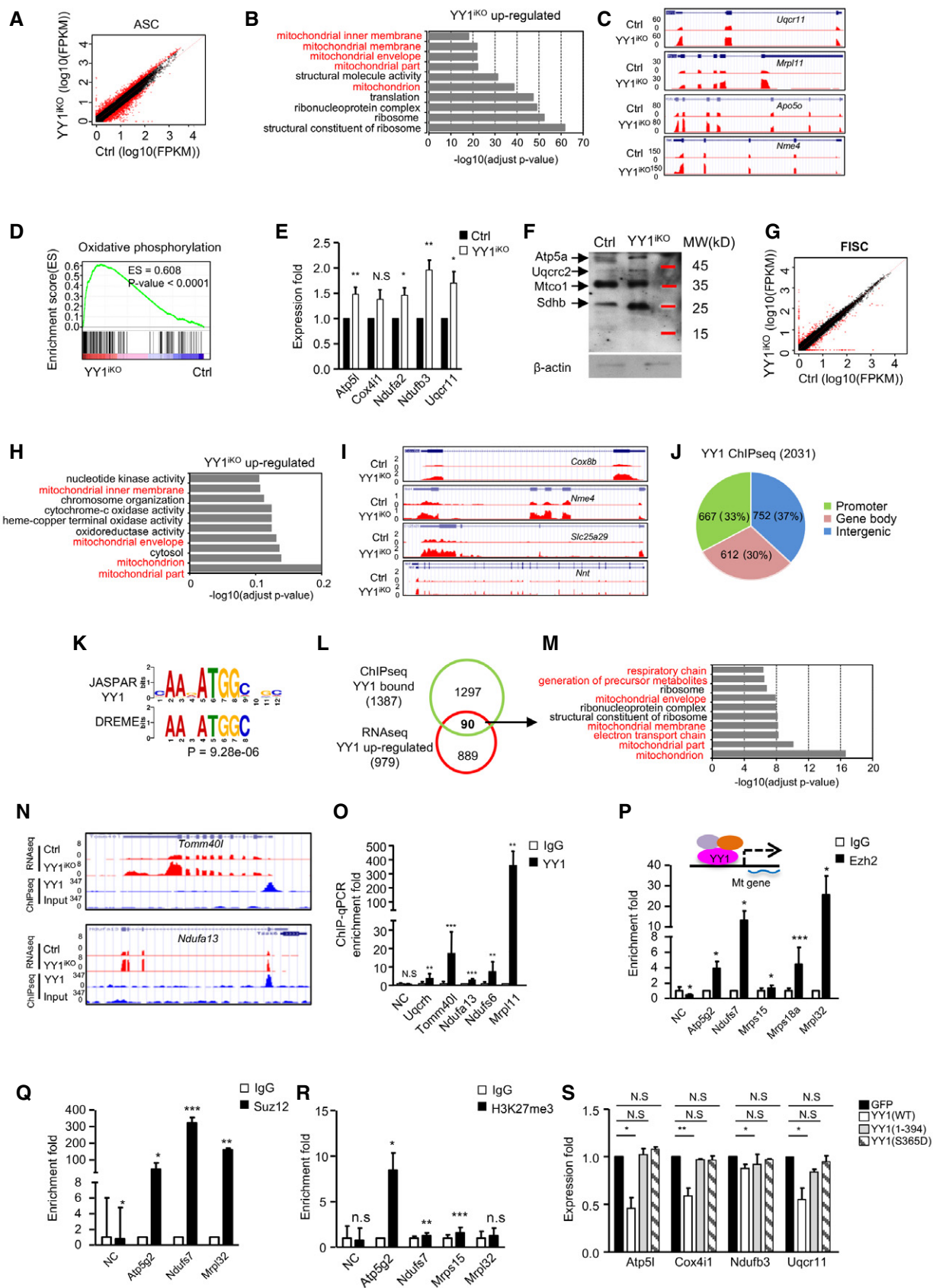


Figure 5.

metabolism; both defects contribute to the delayed activation/proliferation. Indeed, a reduced (22%) level of glucose uptake was found in YY1<sup>IKO</sup> vs. Ctrl (Fig 6D). Also, measurement of the basal extracellular acidification rate (ECAR, a marker of glycolysis) by Seahorse extracellular flux bioanalyzer revealed a 48% decrease in glycolytic usage in YY1<sup>IKO</sup> cells (Fig 6E); this was further strengthened by a reduced (46%) level of lactate production (Fig 6F) as well as an evident decrease (70%) of ATP production (Fig 6G).

To answer what causes the reduced glycolysis in YY1<sup>IKO</sup> cells, analyses of RNAseq data revealed a striking down-regulation of a panel of glycolytic genes even though glycolysis-related terms were not enriched in GO analysis of the 924 down-regulated genes; these genes encode glucose transporters and enzymes involved in virtually every step of glucose metabolism, including *Glut1*, *Hk2*, *Eno1*, *Ldha*, and *Pdk1* (Figs 6H and I, and EV5A and B; Table EV1), suggesting YY1 may modulate the expression of these genes. Indeed, their expressions could be largely rescued by re-expression of WT YY1 in YY1<sup>IKO</sup> cells (Fig 6J). Nevertheless, no direct binding of YY1 was identified on their TSS regions by ChIPseq (Table EV3). To search for plausible mechanisms explaining their down-regulation, we noticed that the majority of these genes, including *Glut1*, *Hk2*, *Gpi*, *Pfkl*, *Pfkfb3*, *Aldoa*, *Eno1*, *Pkm*, *Ldha*, and *Pdk1*, are known trans-activated targets of hypoxia-inducible factor-1 (Hif1 $\alpha$ ; Ito & Suda, 2014), raising an intriguing possibility that the compromised glycolysis in YY1<sup>IKO</sup> cells is mediated by Hif1 $\alpha$ . Xie et al (2018) in fact recently demonstrated the possible induction of Hif1 $\alpha$  in SC proliferation, which nevertheless needs to be confirmed and the exact mechanism behind its involvement in SC, remains unclear. Similar to YY1, an increase in Hif1 $\alpha$  protein was observed in ASCs vs. FISCs (Fig EV5C), suggesting a potential promoting role during SC activation/proliferation. Expectedly, knock-down of Hif1 $\alpha$  reduced the EdU<sup>+</sup> SCs (Fig 6K) and the expression of cell cycle genes as well as glycolytic genes (Fig 6L). Of note, despite the popular notion that hypoxia is a strong driver of Hif1 $\alpha$  expression

through its stabilizing effect, a steady level of Hif1 $\alpha$  protein was detected in ASCs cultured in normoxic condition (21% O<sub>2</sub>; Fig 6M), which could be further stabilized in hypoxic condition (1% O<sub>2</sub>; Fig EV5D). Expectedly, Hif1 $\alpha$  protein level was significantly decreased in YY1<sup>IKO</sup> cells vs. Ctrl by Western blotting (Fig 6M, 54%) and flow cytometric assay (Fig 6N, 26%), suggesting YY1 increases Hif1 $\alpha$  protein levels in ASCs. Consistently, lentiviral re-expression of YY1 in YY1<sup>IKO</sup> cells led to detectable restoration of Hif1 $\alpha$  protein level by flow cytometric assay (Fig 6O).

To answer how YY1 regulates Hif1 $\alpha$ , since no direct binding of YY1 on the Hif1 $\alpha$  promoter/enhancer was detected to suggest a transcriptional regulation, we considered the stabilizing effect of YY1 on Hif1 $\alpha$  protein. Indeed, treatment with cycloheximide (CHX) indicated the degradation rate of Hif1 $\alpha$  protein was much higher (2.23-fold) in YY1<sup>IKO</sup> compared to Ctrl cells (Fig 7A–C). To further ask how YY1 stabilizes Hif1 $\alpha$  protein, we noticed a prior study reported the physical interaction of both proteins in HCT116 cells (Wu et al, 2013). Indeed, by co-immunoprecipitation (Co-IP), a steady interaction was detected between endogenous YY1 and Hif1 $\alpha$  proteins in C2C12 myoblasts in normoxic condition (Fig 7D and E), suggesting YY1 may stabilize Hif1 $\alpha$  through physically interacting with it to prevent its degradation.

To further demonstrate the causative involvement of Hif1 $\alpha$  in the phenotypes of YY1<sup>IKO</sup>, we found that overexpression of a constitutively active form of Hif1 $\alpha$ , HIF1 $\alpha$  (P402A/P564A; Esteban et al, 2006; with double mutations on two prolyl residues, P402A and P564A, to prevent degradation, thus named Hif1 $\alpha$ -DM) in YY1<sup>IKO</sup> cells (Fig EV5E) fully rescued the abundance of glycolytic genes, including *Glut1*, *Gapdh*, *Eno1*, *Pgam1*, *Pkm*, and *Ldha* (Fig 7F). Consequently, cell proliferation was also rescued by EdU labeling assay (Fig 7G). Supportively, overexpression of a wild-type Hif1 $\alpha$  that could not be stabilized failed to rescue the proliferative defect in YY1<sup>IKO</sup> cells (Fig EV5F). Altogether, the above results thus suggested that Hif1 $\alpha$  protein destabilization upon YY1 loss might

#### Figure 6. YY1 loss leads to a defect in glycolytic switch during SC activation via Hif1 $\alpha$ destabilization.

- A An equal number of FACS-isolated SCs from C57 mice were cultured for 24 h and treated with 0, 1, 10, or 20 mM 2-DG (glycolytic inhibitor) or NaN<sub>3</sub> (respiration inhibitor) for 3 h before measurement of ATP production. The relative ATP levels normalized to the 0 mM values are plotted. *N* = 3 mice.
- B SCs from C57 mice were treated with 10 mM 2-DG or 10 mM NaN<sub>3</sub> for 36 h before measurement of proliferation rate by MTS assay (*n* = 3 mice, each).
- C SCs from C57 mice were treated with 10 mM 2-DG for 24 h and subject to EdU labeling for 6 h. The percentage of Pax7<sup>+</sup>/EdU<sup>+</sup> cells over the total number of Pax7<sup>+</sup> cells was quantified (*n* = 3 mice, each).
- D Ctrl and YY1<sup>IKO</sup> ASCs were stained with 60  $\mu$ g/ml 2-NBDG for 45 min, and the fluorescence intensity (MFI) of 2-NBDG was measured by flow cytometry (*n* = 3 mice, each).
- E–G An equal number of Ctrl and YY1<sup>IKO</sup> cells were cultured for 36 h; basal extracellular acidification rate (ECAR) level (E), lactate concentration (F), and ATP production (G) were measured and normalized with cell numbers. *N* = 3 mice.
- H Genomic snapshots depict RNAseq profiles of the selected glycolytic genes (*Hk2*, *Glut1*, *Ldha*, *Pdk1*, and *Eno1*) down-regulated in YY1<sup>IKO</sup> vs. Ctrl ASCs.
- I Expression of the selected glycolytic genes was quantified by RT–qPCR. *Hsp90ab1* was used as the normalization control.
- J Re-expression of YY1 by transfecting YY1<sup>IKO</sup> ASCs with a YY1 WT expressing plasmid led to up-regulation of glycolytic genes including *Glut1*, *Pfkl*, *Gapdh*, *Eno1*, *Pgam1*, and *Pkm*. *Hsp90ab1* was used as the normalization control.
- K FACS-isolated SCs from Pax7-nGFP mice were transfected with Hif1 $\alpha$  or control siRNAs and EdU-labeled for 5 h. The percentage of MyoD<sup>+</sup>EdU<sup>+</sup> cells over the total number of MyoD<sup>+</sup> cells was quantified. Scale bar = 100  $\mu$ m. *N* = 3 mice.
- L The expression of glycolytic genes and cell cycle-related genes was detected by RT–qPCR in the above transfected cells.  *$\beta$ -actin* was used as the normalization control.
- M Hif1 $\alpha$  protein level was detected by Western blotting in YY1<sup>IKO</sup> vs. Ctrl ASCs.  *$\beta$ -actin* was used as the loading control.
- N Left: image of flow cytometric analysis of Hif1 $\alpha$  protein or IgG control in YY1<sup>IKO</sup> vs. Ctrl ASCs. Right: relative mean fluorescence intensity (MFI) of Hif1 $\alpha$  protein is shown. *N* = 3 mice.
- O YY1<sup>IKO</sup> ASCs were transfected with empty YY1 WT viruses; the relative expression level of Hif1 $\alpha$  protein was detected by the above described flow cytometric analysis *N* = 3 mice.

Data information: Error bars represent SD's of the mean. Student's *t*-test (two-sided): N.S = non-significant, \**P* < 0.05, \*\**P* < 0.01, \*\*\**P* < 0.001.

Source data are available online for this figure.

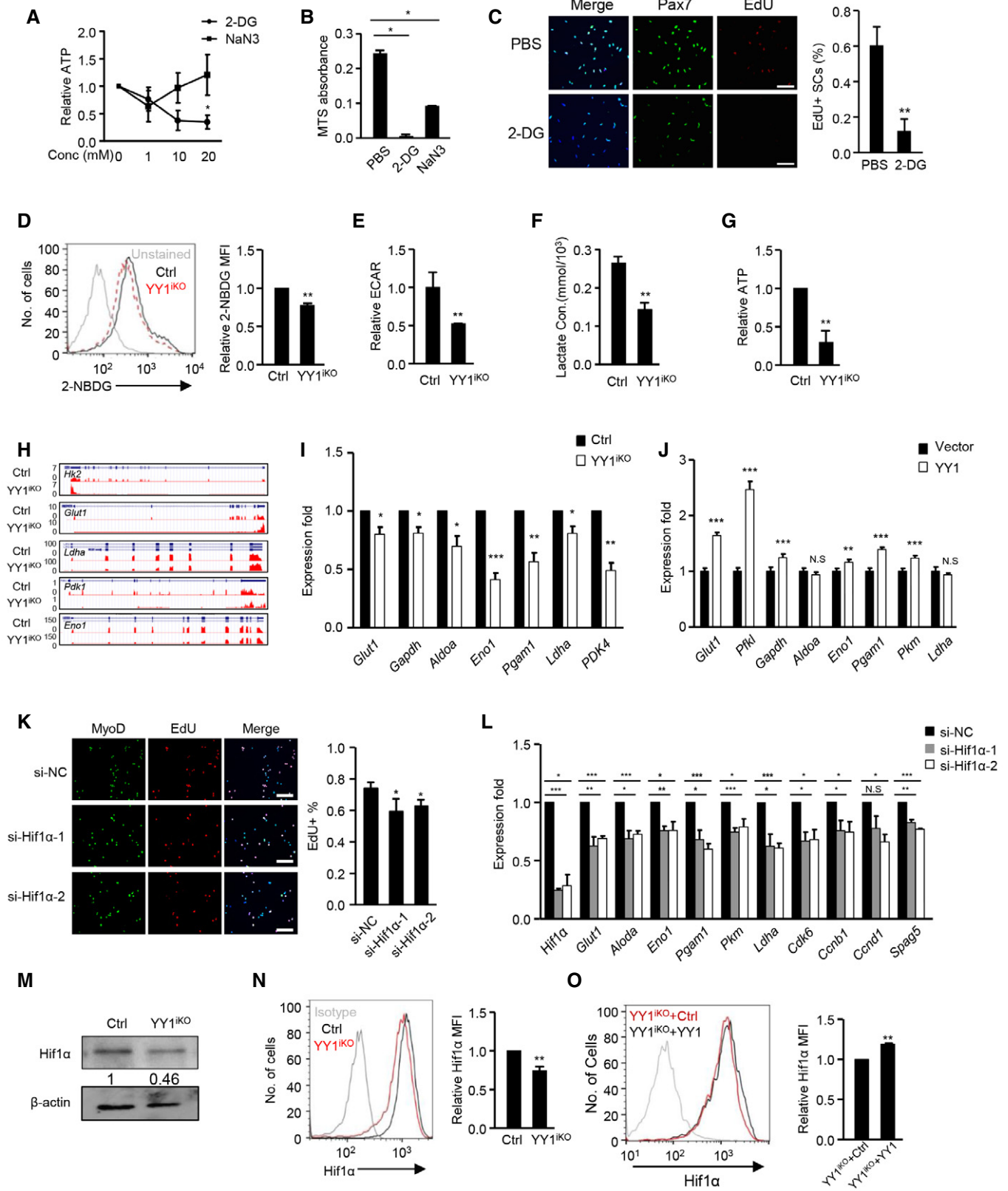


Figure 6.

lead to comprised glycolysis, which partially mediates the proliferation defect seen in YY1<sup>iKO</sup> cells. As suggested by a prior report (Ryall *et al*, 2015), the glycolytic pathway is central to cell proliferation because of its ability to provide building blocks for macromolecule synthesis. Consistently, when examining the RNAseq data closely, we indeed found some pentose cycle enzymes key to nucleotide synthesis were down-regulated (Figs 7H and EV5G). In addition, several genes regulating amino-acid transporters and key to protein synthesis were also down-regulated (Figs 7I and EV5H). To connect the glycolysis with MyoD function, interestingly, we found treatment of 2DG significantly lowered MyoD level (Fig EV5I), indicating glycolysis controls MyoD level. However, re-expression of MyoD in iKO cells failed to rescue the defective proliferation (Fig EV5J and K), suggesting MyoD alone does not mediate YY1 and glycolytic control of cell activation. Altogether, our findings led us to believe that during SCs activation YY1 orchestrates metabolic rewiring through up-regulating Hif1 $\alpha$  which activates many glycolytic genes and simultaneously repressing mitochondrial genes transcriptionally; the dual functions allow it to contribute to the full expansion of SCs. In line with this idea, we found the two YY1 mutant constructs lacking transcriptional activities but possessing protein interacting domain only partially rescued the defective proliferation of YY1<sup>iKO</sup> SCs (Fig 7J and K).

Lastly, it is interesting to mention that despite the marked increase in many mitochondrial genes, measurement of the basal oxygen consumption rate (OCR, an indicator of mitochondrial oxidative activity) by the Seahorse surprisingly revealed a 36% reduction in YY1<sup>iKO</sup> vs. Ctrl ASCs (Fig EV5L). Consistently, MitoTracker labeling of mitochondria in the fixed YY1<sup>iKO</sup> ASCs showed reduced formation of tubular structures characterizing mature mitochondria (Fig EV5M). Quantitative measurement of the mitochondrial membrane potential by staining with JC-1 in living cells also showed a mild (37%) but reproducible decrease (Fig EV5N and O). It is possible that the compromised OXPHOS in YY1<sup>iKO</sup> cells probably resulted from a decreased substrate (pyruvate) flow into mitochondria as a consequence of glycolytic suppression, thus reducing respiratory rate despite the elevated mitochondrial gene levels. In line with this notion, we found treatment of YY1<sup>iKO</sup> cells with sodium pyruvate could partially rescue the decreased mitochondrial activity (Fig EV5N and O).

## Discussion

In this study, we elucidated YY1 function in injury-induced muscle regeneration as well as embryonic muscle development via the use of multiple genetic mouse models. The phenotypic characterization uncovered that ablation of YY1 profoundly impacts the process of regeneration in both acute and chronic injuries as well as the embryonic muscle formation, underscoring the key functions of YY1 in regulating both skeletal muscle regeneration and muscle development. Loss of YY1 caused an intrinsic delay in SC activation and proliferation, which contributes to the severely disrupted regenerative ability in the mutant mouse. Further genome-wide interrogation led to the revelation of YY1 as a crucial factor in controlling metabolic reprogramming during SC proliferation through direct repression of mitochondrial genes transcriptionally and simultaneously enhancing glycolytic pathway via Hif1 $\alpha$  stabilization (Fig 8).

As a TF discovered more than two decades ago, roles of YY1 have been studied in many cellular processes (Gordon *et al*, 2006; He & Casaccia-Bonnel, 2008). Here, we for the first time illuminated its function in regulating adult satellite cell activity in the process of *in vivo* muscle regeneration. The iKO cells in culture displayed an evident reduction in their proliferative rate; the activation step also appeared to be inhibited (Fig 4H–J), underscoring its key function in the very early steps of SC activities. Nonetheless, the lineage progression of FISCs grown in culture did not seem to be blocked as the percentage of Pax7<sup>+</sup>MyoD<sup>+</sup> cells did not differ in Ctrl vs. iKO cells; by 48 h, almost all iKO SCs were MyoD<sup>+</sup> (Fig EV3G). When analyzing the *in vivo* regenerative process, YY1<sup>iKO</sup> mutant mouse, on the other hand, suffered from severe block of regenerative process upon acute injury, suggesting that in addition to the intrinsic delay of SC pool expansion, YY1 deletion may have caused other defects, for example, in SC cross-talking with the niche environment; this warrants further investigation in the future.

To probe into the mechanisms underlying the delayed proliferation in YY1<sup>iKO</sup> cells, we have uncovered a role for YY1 in regulating dual pathways in metabolism. First, mitochondrial gene loci are directly bound and repressed by YY1 genes in a complex with PRC2; this action of YY1 is thus dependent on its transcriptional function, and the mutants lacking DNA-binding activity could not restore the mitochondrial expression in iKO cells (Fig 5S). Notably, several prior

### Figure 7. YY1 stabilizes Hif1 $\alpha$ protein through direct interaction.

- A, B Ctrl or YY1<sup>iKO</sup> ASCs were treated with CHX (cycloheximide) for 90 min, and Hif1 $\alpha$  protein was measured by flow cytometry. The numbers indicate the degradation rate after CHX treatment. *N* = 3 mice.
- C The relative degradation rate was calculated by the ratio of degradation rate in YY1<sup>iKO</sup> (11.14%  $\pm$  1.71%) vs. Ctrl (5.08%  $\pm$  0.796%). *N* = 3 mice.
- D Lysates from C2C12 myoblasts (GM) were subject to co-immunoprecipitation (Co-IP) assays with anti-YY1 or anti-IgG antibodies and blotted with anti-Hif1 $\alpha$  or anti-YY1 antibodies.
- E The above lysates were also immunoprecipitated with anti-Hif1 $\alpha$  or anti-IgG antibodies and blotted with anti-YY1 or anti-Hif1 $\alpha$  antibodies.
- F ASCs from YY1<sup>iKO</sup> mice were infected with pLenti-Hif1 $\alpha$  (P402A/P564A; Hif1 $\alpha$ -DM) viruses to overexpress a non-degradable Hif1 $\alpha$  protein or GFP-expressing viruses. ASCs from Ctrl mice were also infected with the GFP viruses. Thirty-six hours after infection, the expression of target glycolytic genes was detected by RT-qPCR. *Hsp90ab1* was used as the normalization control.
- G SCs were isolated from Ctrl or YY1<sup>iKO</sup> mice and infected with the above viruses. EdU labeling was then performed for 5.5 h. The percentage of MyoD<sup>+</sup>EdU<sup>+</sup> cells over the total number of MyoD<sup>+</sup> cells was quantified. Scale bar = 100  $\mu$ m. *N* = 3 mice.
- H, I Heat maps indicating gene expression levels (Log<sub>2</sub>[FPKM]) of pentose cycle enzymes (H) and amino acid transporter (I) in YY1<sup>iKO</sup> vs. Ctrl.
- J, K YY1 (S365D) (J) or YY1 (1-394) (K) mutant was expressed in YY1<sup>iKO</sup> ASCs and cells were then EdU-labeled for 6 h. A GFP-expressing plasmid was used as the negative control. The percentage of Pax7<sup>+</sup>/EdU<sup>+</sup> cells over the total number of Pax7<sup>+</sup> cells was quantified.

Data information: Error bars represent SD's of the mean. Student's *t*-test (two-sided): N.S = non-significant, \**P* < 0.05, \*\**P* < 0.01, \*\*\**P* < 0.001. Source data are available online for this figure.

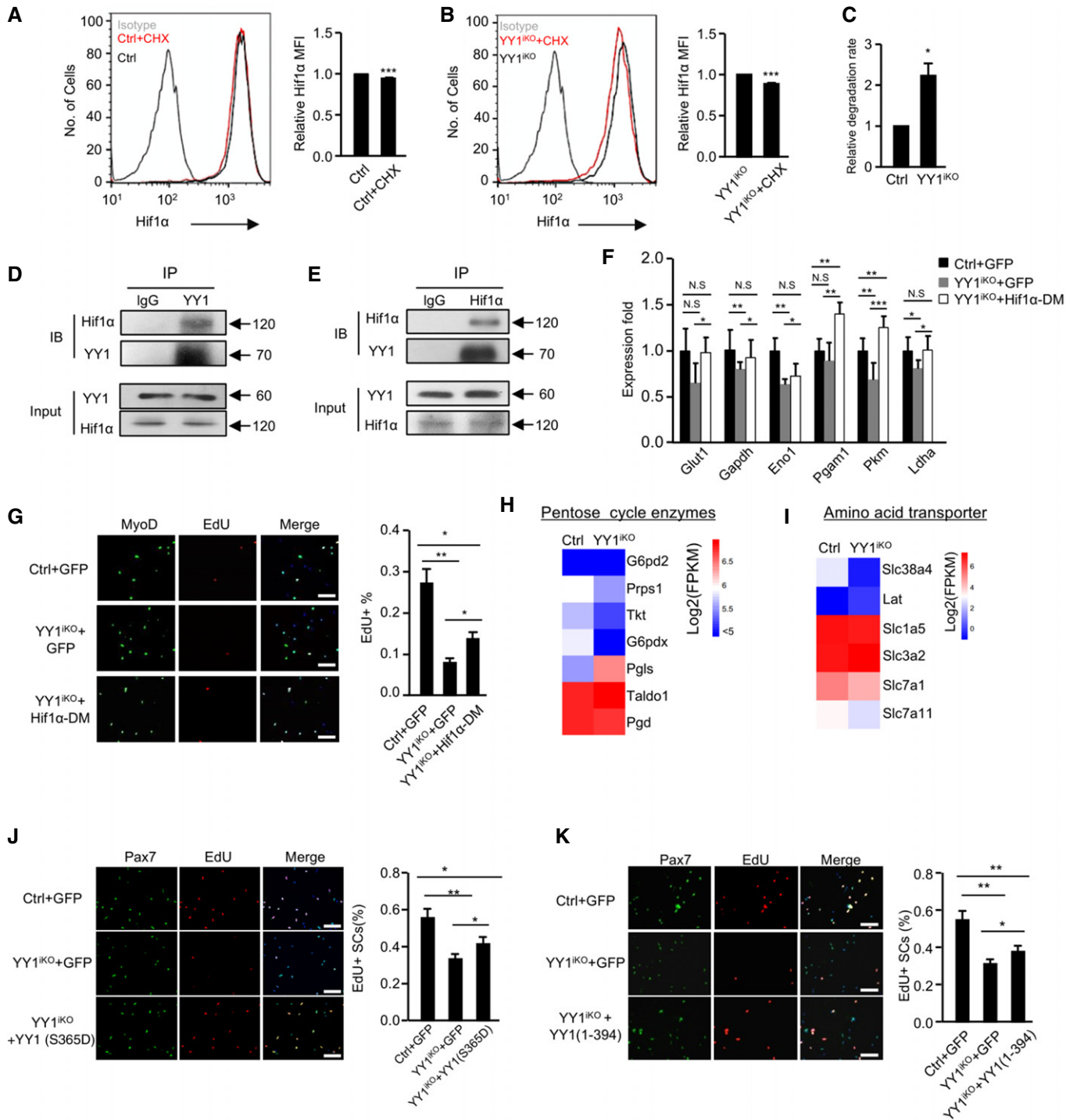
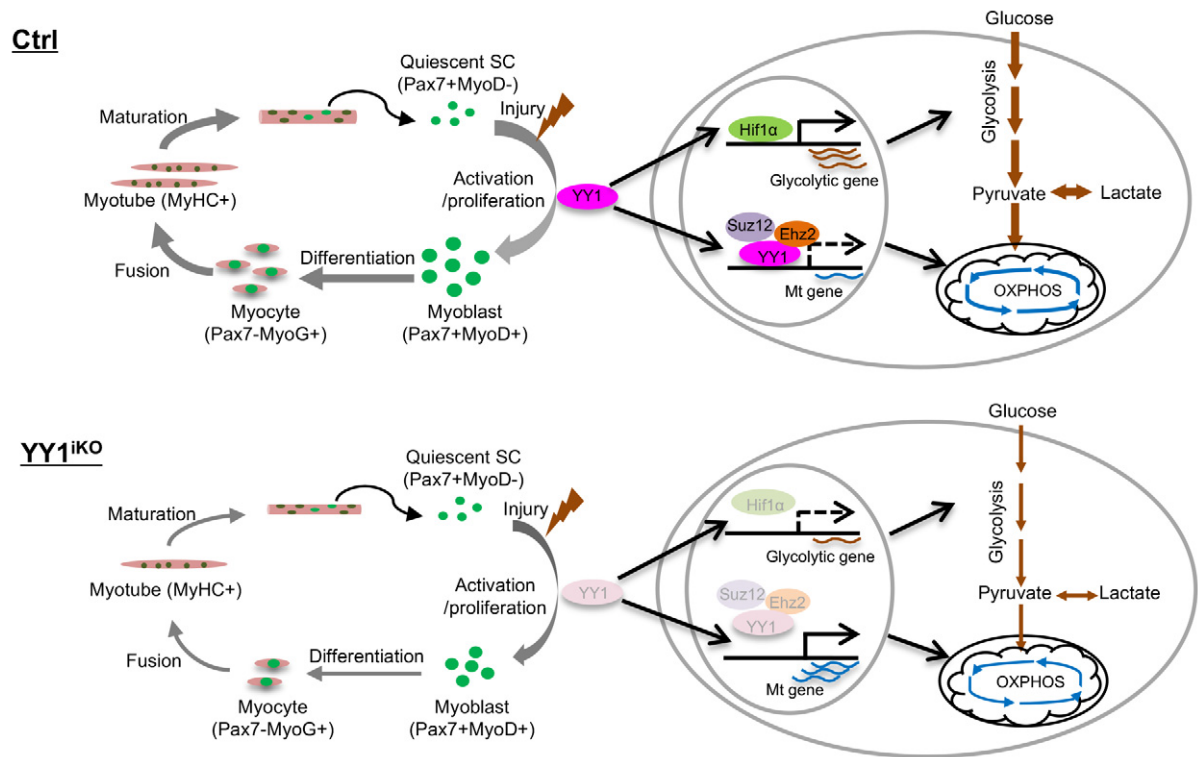


Figure 7.

studies have shed light on the important regulatory roles of YY1 in mitochondrial function and oxidative phosphorylation in various cells. For example, Blattler *et al* (2012) demonstrated that skeletal muscle tissue-specific YY1 KO mice have severely defective mitochondria morphology and oxidative function associated with exercise intolerance. Perekatt *et al* (2014) also disclosed that YY1 is essential for intestinal stem cell renewal; loss of YY1 promotes the intestinal

stem cells to exist from their niche and proliferation of the cells is unaffected. Very interestingly, in contrast to our findings, YY1 was found to be an activating factor for mitochondrial genes and functions in these studies. For example, in intestinal stem cells YY1 binds to mitochondrial complex I genes and is required for their expression; mitochondrial structure and function are compromised upon YY1 loss (Perekatt *et al*, 2014). These rather opposing findings suggest





**Figure 8. Schematic model of the role of YY1 during adult muscle regeneration.**

YY1 controls the activation of SCs by acting as a switch of metabolic reprogramming. In Ctrl SCs, its expression is increased during SC activation upon injury-induced muscle damage and it transcriptionally suppresses mitochondrial gene expression through direct binding to their TSS regions together with PRC2 repressive complex. Meanwhile, it also stabilizes Hif1 $\alpha$  protein to facilitate its trans-activating of glycolytic genes. As a result, successful activation of glycolytic pathways occurs, allowing SCs to activate and proliferate to drive the repairing of the damaged muscle. When YY1 is deleted in the YY1<sup>iKO</sup> mouse, Hif1 $\alpha$  level is decreased due to protein destabilization, leading to a reduction in glycolytic gene expression and glycolytic rate. Meanwhile, although the expression of mitochondrial genes is up-regulated, OXPHOS could not be increased possibly because of reduced flow of pyruvate substrate into mitochondria. As a result of the inhibited metabolic reprogramming, SC activation is repressed and the regeneration is compromised. Quiescent SCs are defined by expression of Pax7 and lack of MyoD expression (Pax7<sup>+</sup>MyoD<sup>-</sup>), activated and proliferating myoblasts by the concomitant expression of Pax7 and MyoD (Pax7<sup>+</sup>MyoD<sup>+</sup>), differentiating myocytes by expression of MyoG (Pax7<sup>-</sup>MyoG<sup>+</sup>), and differentiated myotubes are marked by expression of Myosin heavy chain (MyHC). Error bars represent SD's of the mean. Student's *t*-test (two-sided): \**P* < 0.05, \*\**P* < 0.01, \*\*\**P* < 0.001.

that YY1 binding to mitochondrial genes can cause pleiotropic regulatory effects depending on the cellular context. Considering the ubiquitous expression of YY1 in many types of stem cells, we suspect it can act as a key TF regulating mitochondrial function in linking stem cell metabolism to their lineage progression.

In addition to directly controlling the expression of mitochondrial genes, we for the first time showed that YY1 could also modulate glycolytic pathway through stabilizing Hif1 $\alpha$  protein, thus underpinning YY1 as a metabolic controller with dual functions simultaneously modulating two main bioenergetic pathways to facilitate the proliferative growth of SCs. Hif1 $\alpha$  is emerging as a key regulator of glycolysis via direct trans-activation of many glycolytic genes (Ito & Suda, 2014); here, we for the first elucidated its functionality and mechanism in regulating SC metabolism and extended findings from two prior reports (Yang *et al.*, 2017; Xie *et al.*, 2018). In the study by Yang *et al.*, when both Hif1 $\alpha$  and Hif2 $\alpha$  genes were deleted by Pax7CreER, an obvious delay was observed during CTX injury-induced muscle regeneration (Fig 4); nevertheless, no single mutant was made to further investigate their separate roles. In the more recent report by Xie *et al.* studying Hif2 $\alpha$  functionality, overexpression of Hif1 $\alpha$  in SCs was shown to promote cell proliferation

although no further mechanistic insight was provided. We showed that YY1 regulation of Hif1 $\alpha$  most likely occurs through the physical interaction of both proteins, which is independent of its transcriptional activity (Fig 7D and E). It is also interesting to point out that our dissection of YY1-Hif1 $\alpha$  connection in SCs was mainly conducted in a normoxic condition, leading to the unexpected finding that YY1 can stabilize Hif1 $\alpha$  protein in normoxia. In contrast to the common belief that Hif1 $\alpha$  function is dependent on hypoxia, the normoxic Hif1 $\alpha$  protein appears to exert an important function in regulating SC activation. During the course of the preparation of this manuscript, Wu *et al.* (2018) recently reported that YY1 alters tumor cell metabolism by activating glucose-6-phosphate dehydrogenase (G6PD), which is in line with our finding; nonetheless, the YY1 activation of G6PD was shown to be directly at transcriptional level, distinct from the mechanism presented in our study.

Taken together, our study demonstrates that YY1 plays dual roles in suppressing mitochondrial genes and increasing Hif1 $\alpha$  to facilitate a smooth activation of glycolytic pathway that is needed for SC activation/proliferation. Interestingly, although its function in the proliferative stage appears to repress mitochondrial activation and to enhance glycolysis, it becomes an activator of

mitochondrial genes and oxidative phosphorylation in the differentiation stage according to Blattler *et al* (2012). This is reminiscent of a recent report showing YY1 activates genes involved in mitochondrial bioenergetics in B cells (Kleiman *et al*, 2016). This duality of YY1 function thus renders YY1 a key regulator of metabolic remodeling driving the entire SCs lineage progression from activation to differentiation. This seemingly opposite regulatory abilities on mitochondrial genes stem from its competence to form distinct co-repressive or co-activating complexes at different stages. Specifically, we found that YY1 and PRC2 synergistically repress mitochondrial loci in ASCs, while PGC1 $\alpha$  was shown to be recruited by YY1 to increase mitochondrial genes in skeletal muscle tissue (Cunningham *et al*, 2007). To summarize, our findings demonstrated that this metabolic reprogramming orchestrated by YY1 plays a direct role in controlling stem cell fate. Better deciphering the interplay between bioenergy and stem cell differentiation should improve our ability to manipulate stem cells *in vitro*, which is of great interest for the development of regenerative medicine (Chen & Chan, 2017; Schell *et al*, 2017).

## Materials and Methods

### Animal studies

Pax7<sup>Cre</sup> (Keller *et al*, 2004), Pax7<sup>CreERT2/+</sup> (Lepper *et al*, 2009), and Tg: Pax7-nGFP mouse strains (Sambasivan *et al*, 2009) were kindly provided by Dr. Shahragim Tajbakhsh. YY1<sup>f/f</sup> (Affar el *et al*, 2006) and C57BL/10 ScSn DMDmdx (mdx) mouse strains were purchased from The Jackson Laboratory (Bar Harbor, ME, USA). The YY1 conditional KO (YY1<sup>CKO</sup>) strain (Ctrl: Pax7<sup>+/+</sup>; YY1<sup>f/f</sup>, YY1<sup>CKO</sup>: Pax7<sup>Cre/+</sup>; YY1<sup>f/f</sup>) was generated by crossing Pax7<sup>Cre</sup> mice with YY1<sup>f/f</sup> mice. The YY1-inducible conditional KO (YY1<sup>iKO</sup>) strain (Ctrl: Pax7<sup>CreERT2/+</sup>; YY1<sup>+/+</sup>, YY1<sup>iKO</sup>: Pax7<sup>CreERT2/+</sup>; YY1<sup>f/f</sup> mice) was generated by crossing Pax7<sup>CreERT2/+</sup> mice with YY1<sup>f/f</sup> mice. The YY1/mdx double KO (YY1<sup>dKO</sup>) strain (Ctrl: Pax7<sup>CreERT2/+</sup>; YY1<sup>+/+</sup>; Mdx, YY1<sup>dKO</sup>: Pax7<sup>CreERT2/+</sup>; YY1<sup>f/f</sup>; Mdx) was generated by crossing YY1<sup>iKO</sup> with mdx mice. Primers used for genotyping are shown in Table EV4. Inducible conditional deletion of YY1 was administered by tamoxifen (TM; T5648, Sigma) intraperitoneally (IP) at 2 mg per 20 g body weight. For cardiotoxin (CTX) studies, approximately 2-month-old mice were injected with 50  $\mu$ l of 10  $\mu$ g/ml CTX (Latoxan, France) solution into TA muscles. Muscles were harvested at designated time points for further analysis. All animal handling procedures and protocols were approved by the Animal Ethics Committee at Chinese University of Hong Kong (CUHK). For EdU incorporation assay *in vivo*, 2 days after CTX injection, EdU injection via intraperitoneally (IP) at 0.25 mg per 20 g body weight was performed, followed by FACS isolation of SCs 12 h later. Cells were then collected and fixed with 4% PFA. EdU-labeled cells were visualized using “click” chemistry with an Alexa Fluor® 594-conjugated azide. Pictures were captured with a fluorescence microscope (Leica).

### *In vitro* muscle functional test

The test was performed according to previous method (Zhang *et al*, 2016). Dissected EDL/SOL muscles with intact tendons were

mounted into warmed 95% O<sub>2</sub>/5% CO<sub>2</sub>-bubbled Krebs solution. One tendon was attached to a force transducer (In Vitro Muscle Test System 1200, Aurora Scientific Inc., Aurora, ON, Canada); the other end was tied to a hook connected to the lever arm of a position feedback motor. The optimum length (L<sub>0</sub>) was adjusted based on the maximal twitch force. Muscles were stimulated with supramaximal intensity at 100 Hz for 400 ms for tetanic force measurements. Specific tetanic force values were calculated by peak tetanic force normalized to the muscle physiological CSAs (PCsAs).

### Cell culture

Mouse C2C12 myoblast cells (CRL-1772) and 293 T cells were obtained from ATCC and cultured in DMEM medium (12800-017, Gibco) with 10% fetal bovine serum (10270-106, Gibco), penicillin/streptomycin (1 $\times$ ; 15140-122, Gibco) at 37°C in 5% CO<sub>2</sub> incubator. SCs were cultured in F10 medium (F0723, Merck Millipore) with 20% fetal bovine serum, penicillin/streptomycin (1 $\times$ ), and 2.5 ng/ml basic fibroblast growth factor (13256, Life Technologies). To induce SCs differentiation, cells were switched to F10 medium with 2% horse serum (126050088, Invitrogen). To inhibit protein degradation, SCs were treated with 6  $\mu$ M MG132 (M8699, Sigma) for 2 h. To inhibit protein synthesis, SCs were treated with 100  $\mu$ g/ml cycloheximide for 90 min. To provide alternate carbon substrate to YY1<sup>iKO</sup> cells, SCs were treated with 100  $\mu$ M sodium pyruvate (11360070, Thermo Fisher) for 24 h. For hypoxic treatment, cells were exposed to hypoxia *in vitro* in New Brunswick™ Galaxy® 48 S incubator (MG Scientific, USA) with 1% oxygen for indicated time. Transient transfection of plasmids or siRNA was conducted with Lipofectamine 2000 (11668-019, Invitrogen) following manufacturer's protocol. For viral infection, pRlenti-GFP or pRlenti-Hif1 $\alpha$  (P402A/P564A; Hif1 $\alpha$  double mutant or Hif1 $\alpha$ -DM), pSL5 or pSL5/YY1 along with the packaging plasmids was transfected into HEK293T cells. Forty-eight hours after transfection, culture supernatant was collected and used for infecting SCs. To investigate the effect of p38 signaling on mitochondrial genes, cells were treated with 10  $\mu$ M SB202190 (S7076, Sigma) for 24 h (Wang *et al*, 2018).

### FACS isolation of SCs

SCs were sorted based on established methods (Cheung *et al*, 2012). Briefly, hindlimb muscles from mice were digested with collagenase II (800 units/ml) for 90 min at 37°C, and then digested muscles were triturated and washed in washing medium [Hams F-10 media (Gibco), 10% HHS (Gibco), penicillin/streptomycin (1 $\times$ , Gibco)] before SCs were liberated by treating with collagenase II (800 units/ml)/dispase (11 unit/ml) for 30 min. Mononuclear cells were filtered with a 45-mm cell strainer and incubated with primary antibodies (Vcam1-biotin, CD31-fluorescein isothiocyanate [FITC], CD45-FITC, and Sca1-Alxa647). The Vcam1 signal was amplified with streptavidin-PE-cy7. All antibodies were used at a dilution of 1:75. The BD FACSAria IV cell sorter (BD Biosciences) was used for SC sorting following the manufacturer's instructions.

### Myofiber isolation

As described before (Zhou *et al*, 2015; Chen *et al*, 2017), extensor digitorum longus (EDL) muscles were dissected and digested with

Collagenase II (800 units/ml) in DMEM media (Gibco) at 37°C for 75 min. Single myofibers were released by gentle trituration with washing medium (mentioned above). Fibers were cultured in Ham's F10 medium with 10% HS and P/S (1×) or Ham's F10 medium supplemented with 10% FBS and 2.5 ng/ml basic fibroblast growth factor at designated time points. Fixation was carried out in 4% paraformaldehyde at room temp for 15 min.

### Cell proliferation assay

EdU assay was conducted following manufacturer's instructions (C10339, Thermo Scientific). Growing cells on coverslips were incubated in culture medium with 10 μM EdU for designated times. Cells were then washed for three times in PBS and fixed with 4% PFA for 20 min. EdU-labeled cells were visualized using "click" chemistry with an Alexa Fluor® 594-conjugated azide. Pictures were captured with a fluorescence microscope (Leica). MTS assay was conducted using CellTiter 96® Aqueous One Solution Reagent (Promega, Madison, WI) following the manufacturer's instructions. Briefly, cells were seeded at a density of  $10 \times 10^3$  cells/well (SCs) in a 96-well plate and cultured for 12 h, followed by treatment of 10 mM 2-DG/NaN<sub>3</sub> for 36 h. The proliferation was measured with absorbance at 490 nm with background subtraction at 650 nm.

### TUNEL assay

TUNEL assays to monitor apoptosis were carried out with the *In Situ* Cell Death Detection Kit (Roche) according to the manufacturer's protocol. Briefly, freshly isolated cells on coverslips were cultured for 36 h, followed by washing twice in PBS and fixing with 4% PFA for 15 min. TUNEL staining was carried out by adding reaction mixture of label solution and enzyme solution for 60 min at dark. Fluorescent images were captured with a fluorescence microscope (Leica).

### Cellular bioenergetics

Cellular bioenergetics was analyzed on a Seahorse extracellular flux bioanalyzer (XF24) based on previously described methods (Ryall *et al*, 2015). Briefly, cells were seeded at a density of  $50 \times 10^3$  cells/well (SCs) in a Seahorse XF24 plate. Cells were cultured for 36 h in growth media. Immediately prior to the assay, cultured cells were washed twice in minimal assay media (Seahorse Biosciences, 37°C, pH 7.40) supplemented with 25 mM glucose and 1 mM sodium pyruvate. All cells were equilibrated in minimal assay media for 1 h in a non-CO<sub>2</sub> incubator immediately prior to the assay. The basal rate of extracellular acidification rate (ECAR) was measured in triplicate for 2 min (over a total of 15 min) from the rate of decline in O<sub>2</sub> partial pressure (OCR) and rate of change in assay pH (ECAR).

### Lactate assay

The lactate level in cell supernatant was measured using the Lactate Assay Kit (1200011002, Eton Bioscience, USA) according to the manufacturer's instructions. Briefly, cells were seeded at a density of  $20 \times 10^3$  cells/well (SCs) in a 96-well plate and cultured for 40 h, and the cell culture supernatant was then collected and mixed with

L-Lactate assay solution for 30 min at 37°C incubator. The concentration of L-Lactate was measured with an absorbance at 490 nm.

### Measurement of glucose uptake

Briefly, cells were seeded at a density of  $20 \times 10^4$  cells/well (SCs) in a 12-well plate and cultured for 36 h. Cells were then rinsed twice with NO-glucose medium with 20% FBS and incubated with 60 μg/ml 2-NBDG for 45 min. Trypsinized cells were then analyzed by flow cytometer BD FACSAria Fusion (BD Biosciences). Raw data were analyzed by FlowJo software.

### MitoTracker fluorescence staining

MitoTracker®Red CMXRos (M7512, Invitrogen) was added into growth media of SCs at a final concentration of 10 nM for 3 min, followed by washing with PBS and fixing the cells with 4% paraformaldehyde. Images were visualized by 100× oil lens of a fluorescence microscope (Leica).

### Measurement of mitochondrial membrane potential

Briefly, SCs were seeded at a density of  $20 \times 10^4$  cells/well in a 12-well plate and cultured for 36 h. Trypsinized cells were stained with 2 μM 5,5',6,6'-tetrachloro-1,1',3,3'-tetraethyl-benzimidazolylcarbocyanine chloride (JC-1; Invitrogen) and analyzed by flow cytometer FACSCanto II Analyzer (BD Biosciences). Raw data were analyzed by FlowJo software.

### ATP measurement

ATP concentrations in cells were determined luminometrically using an ApoSENSOR™ Cell Viability Assay Kit (K254, Biovision, USA) according to the manufacturer's instructions. Briefly, cells were seeded at a density of  $10 \times 10^3$  cells/well (SCs) in a 96-well plate and cultured for 36 h. Cells were lysed with Nuclear Releasing Buffer for 5 min; 10 μl ATP Monitoring Enzyme was added to the cell lysate, and the concentration of ATP was measured with a luminometer (PerkinElmer).

### Plasmids

The full-length YY1 expression plasmid was described before (Wang *et al*, 2008). The full-length Myod expression plasmid was described before (Skapek *et al*, 1996). pRlenti-GFP or pRlenti-Hif1α (P402A/P564A; carrying the following substitutions: P402A and P564A) was a kind gift from Prof. Miguel Esteban (GIBH, Guangzhou, China; Esteban *et al*, 2006). pSL5 or pSL5/YY1 was a kind gift from Prof. Guangchao Sui (NEFU, Harbin, China; Wan *et al*, 2012). pRlenti-YY1 (1–394) and pRlenti-YY1 (S365D) expressing vector were constructed by PCR amplification from pCEP4F-YY1(1–399) or pCS2 (+)Flag-YY1(S365D), following by T–A cloning into pRlenti-GFP using BamH I and EcoR I sites.

### Real-time PCR

Total RNAs from satellite cells were extracted using TRIzol reagent (Life Technologies) according to the manufacturer's protocol.

Real-time PCR was performed by using SYBR Green Master Mix (Applied Biosystem) on ABI PRISM 7900HT (Applied Biosystem). HSP90 was used for normalization. All the experiments were designed in triplicates. Primers used for RT-qPCR are shown in Table EV4.

### Immunoblotting, immunofluorescence, and immunohistochemistry

For Western blot assays, *in vitro* cultured cells were harvested, washed with ice-cold PBS, and lysed in cell lysis buffer. Whole-cell lysates were subjected to SDS-PAGE, and protein expression was visualized using an enhanced chemiluminescence detection system (GE Healthcare, Little Chalfont, UK) as described before (Wang *et al*, 2007). The following dilutions were used for each antibody: YY1 (Santa Cruz Biotechnology; 1:1,000),  $\alpha$ -tubulin (Sigma; 1:5,000), Hif1 $\alpha$  (Abcam; 1:1,000),  $\beta$ -actin (ImmunoWay; 1:5,000), and OXPHOS Rodent WB Antibody Cocktail (Abcam, 1:250). For immunofluorescence staining, cultured cells and myofibers were fixed in 4% PFA for 15 min and blocked with 3% BSA within 1 h. Primary antibodies were applied to samples with indicated dilution below, and the samples were kept at 4°C overnight. For Pax7 staining on frozen muscle sections, an antigen retrieval step was performed before blocking through boiling samples in 0.01 M citric acid (pH 6.0) for 5 min in a microwave. After 4% BBBSA (4% IgG-free BSA in PBS; Jackson, ref: 001-000-162) blocking, the sections were further blocked with the donkey anti-mouse IgG (H + L; 1/100 in PBS; Jackson, ref: 115-007-003) for 30 min. The biotin-conjugated anti-mouse IgG (1:500 in 4% BBBSA, Jackson, ref: 115-065-205) and Cy3-Streptavidin (1:1,250 in 4% BBBSA, Jackson, ref: 016-160-084) were used as secondary antibodies. H&E staining on frozen muscle sections was performed as previously described (Diao *et al*, 2012). Masson's trichrome staining was performed according to the manufacturer's instructions (ScyTek Laboratories, Logan, UT). All fluorescent images were captured with a fluorescence microscope (Leica). Primary antibodies used include the following: YY1 (1:100) for staining of isolated SCs (Santa Cruz Biotechnology, Inc), MyoD (1:100; Santa Cruz Biotechnology, Inc), and myogenin (1:200; Santa Cruz Biotechnology, Inc); Pax7 (1:100; Developmental Studies Hybridoma Bank) and MF20 (1:50; Developmental Studies Hybridoma Bank); troponin (1:200; Sigma-Aldrich), MyHC (1:200; Sigma-Aldrich), and laminin (1:800; Sigma-Aldrich); Ki67 (1:200; Thermo); collagen I (1:200; Southern Biotech); MyoD (1:200; Dako); and Hif1 $\alpha$  (1:200; Abcam) and YY1 (1:200; Abcam) for staining of muscle cryosections.

### Flow cytometric analysis of protein levels

SCs were collected by incubation with 0.5% trypsin, fixed by using 4% PFA for 15 min at RT, and then permeabilized with treatment of 90% ice-cold methanol. After blocking with 1% BSA for 30 min at RT, cells were stained with a rabbit anti-Hif1 $\alpha$  (Abcam, ab2185) or a rabbit anti-YY1 (Santa Cruz Biotechnology, sc-1703) or anti-rabbit IgG control (Jackson ImmunoResearch Laboratories) for 45 min at 4°C. Cells were then stained with Alexa Fluor® 594-conjugated goat anti-rabbit secondary antibody (Thermo Fisher Scientific, R37117) for 15 min at 4°C and analyzed by flow

cytometer BD FACSAria Fusion (BD Biosciences). Raw data were analyzed by FlowJo software.

### Co-immunoprecipitation assay

C2C12 cells were cross-linked with 200  $\mu$ g/ml of 3,3'-Dithiodipropionic acid di(N-hydroxysuccinimide ester) (Sigma) for 15 min and then harvested and lysed in RIPA buffer (25 mM HEPES pH 7.4, 1% nonidet P-40, 0.1% SDS, 0.5% sodium deoxycholate, 1  $\times$  PIC). 5  $\mu$ g of antibodies against YY1 (Santa Cruz Biotechnology, Cat# SC-1703, rabbit polyclonal), Hif1 $\alpha$  (Santa Cruz Biotechnology, Cat# SC-10790, rabbit polyclonal), or normal mouse IgG (Santa Cruz Biotechnology, Cat# SC-2025) was incubated with above cell lysate overnight at 4°C with rotation. After extensive washing with RIPA buffer, the bound proteins were eluted by boiling in 50  $\mu$ l of 1  $\times$  loading buffer (125 mM Tris-HCl pH 6.8, with 4% SDS, 20% (v/v) glycerol) and subjected to Western blotting analysis.

### ChIP assays

Ten million SCs were cultured for 36 h and subsequently cross-linked in 1% formaldehyde and processed according to previously described (Lu *et al*, 2012; Zhou *et al*, 2012b; Peng *et al*, 2017). In all, 5  $\mu$ g of antibodies against YY1 (Santa Cruz Biotechnology, Cat# SC-1703, rabbit polyclonal), Ezh2 (Active Motif, Cat# 61642, rabbit polyclonal), Suz12 (Abcam, Cat# 12073, rabbit polyclonal), H3K27me3 (Millipore, Cat# 07-449, rabbit polyclonal), or normal mouse IgG (Santa Cruz Biotechnology, Cat# SC-2025) was used for one immunoprecipitation. Immunoprecipitated genomic DNA was resuspended in 20  $\mu$ l of water. PCRs were performed with 1  $\mu$ l of immunoprecipitated material as a template and products were analyzed by qRT-PCR on a 7900HT system (Life Technologies). Relative enrichment is calculated as the amount of amplified DNA from ChIP group relative to values from IgG group. Primers used for ChIP-qPCR are shown in Table EV4.

### ChIP sequencing and data analysis

For library construction, we used a protocol as described before (Lu *et al*, 2013; Zhou *et al*, 2015; Peng *et al*, 2017). Briefly, the purified DNA (100 ng) was end-repaired, and A-nucleotide overhangs were added by incubation with the Taq Klenow fragment lacking exonuclease activity. After the attachment of anchor sequences, fragments were PCR-amplified using Illumina-supplied primers. The purified DNA library products were evaluated using Bioanalyzer (Agilent) and SYBR qPCR and diluted to 10 nM for sequencing on Illumina HiSeq 2000 sequencer (YY1; pair-end with 50 bp). A data analysis pipeline CASAVA 1.8 (Illumina) was employed to perform the initial bioinformatics analysis including base calling and converting the results into raw reads in FASTQ format. For peak defining, the sequenced reads were mapped to the mouse reference genome (mm9) using bowtie2 (Langmead & Salzberg, 2012). The alignment was performed, and only the uniquely aligned reads were kept. The protein DNA-binding peaks (sites) were identified using model-based analysis for ChIPseq (MACS, version 2.1.1; Zhang *et al*, 2008) with input sample as the background. During the peak calling, the *P*-value cutoff was set to under 0.0001 for YY1 ChIPseq experiment.

## RNAseq and data analysis

For library construction, we used a protocol as described before (Lu *et al*, 2013; Zhou *et al*, 2015). The purified library products were evaluated using a Bioanalyzer (Agilent) and SYBR qPCR and sequenced on an Illumina HiSeq 2000 sequencer (pair-end with 50 bp). Sequenced fragments were mapped to reference mouse genome (mm9) using TopHat2 (Kim *et al*, 2013). Cufflinks (Trapnell *et al*, 2012) were then used to estimate the relative abundance of transcripts in RNAseq experiments. Abundances were reported in fragments per kilobase per million (FPKM), which is conceptually analogous to the reads per kilobase per million (RPKM) used for single-end RNAseq. Differentially expressed genes were identified if the fold change  $\geq 2$  by comparing YY1<sup>ikO</sup> and Ctrl samples.

## Statistical test

The statistical significance was assessed by the Student's *t*-test (two-sided). \* $P < 0.05$ , \*\* $P < 0.01$ , \*\*\* $P < 0.001$  and n.s.: not significant ( $P \geq 0.05$ ).

## Data availability

RNAseq and ChIPseq data used in this study have been deposited in Gene Expression Omnibus (GEO) database under the accession codes GSM2893681, GSM2893682, GSM2893683, GSM2893684, GSM2893685, and GSM2893686.

**Expanded View** for this article is available online.

## Acknowledgements

We thank Prof. Miguel Esteban for sharing the Hif1 $\alpha$ (P402A/P564A) plasmid; Prof. Guangchao Sui for sharing pSL5/YY1 plasmid; Prof. Raed Rizkallah for sharing pCS2(+)/Flag-YY1(S365D) plasmid; Dr. James G. Ryall for advice on cellular bioenergetics; Prof. Gabrielle Kardon for their technical assistance on handling mouse embryos; Dr. Han Zhu for his suggestions on fluorescence-activated cell sorting (FACS). We thank General Research Funds (GRF) from the Research Grants Council (RGC) of the Hong Kong Special Administrative Region (Project Code: 14100415, 14133016, 14106117, and 14100018 to H.W.; 14102315 and 14116918 to H.S.); CUHK Focused Innovations Scheme: Scheme B to H.S. (Project Code: 1907307); National Natural Science Foundation (NSFC) of China (Grant No: 31871304 to H.W.); NSFC/RGC Joint Research Scheme from RGC (Project Code: N\_CUHK413/18 to H.S.). Direct Grant from CUHK (Project Number: 2017.049 to H.W. and 2017.009 to H.S.). This work was also supported by the Hong Kong Epigenomics Project (EpiHK).

## Author contributions

HW and HS conceived the projects, designed the experiments, and wrote the manuscript. FC conducted most of the experiments. JZ analyzed RNAseq and ChIPseq data. YL, YC, LW, ZZ, CCW, and BZ helped to perform some of the mouse assays. CC-LW helped to perform assays of measuring mitochondrial membrane potential. JY provided help on the analysis of fiber size. YZ helped to review and edit the manuscript. ZW and THC provided suggestions on some satellite cell experiments.

## Conflict of interest

The authors declare that they have no conflict of interest.

## References

- Affar el B, Gay F, Shi Y, Liu H, Huarte M, Wu S, Collins T, Li E (2006) Essential dosage-dependent functions of the transcription factor yin yang 1 in late embryonic development and cell cycle progression. *Mol Cell Biol* 26: 3565–3581
- Alexander KE, Rizkallah R (2017) Aurora A phosphorylation of YY1 during mitosis inactivates its DNA binding activity. *Sci Rep* 7: 10084
- Aziz A, Sebastian S, Dilworth FJ (2012) The origin and fate of muscle satellite cells. *Stem Cell Rev* 8: 609–622
- Babiuk RP, Zhang W, Clugston R, Allan DW, Greer JJ (2003) Embryological origins and development of the rat diaphragm. *J Comp Neurol* 455: 477–487
- Bentzinger CF, Wang YX, Rudnicki MA (2012) Building muscle: molecular regulation of myogenesis. *Cold Spring Harb Perspect Biol* 4: a008342
- Blattler SM, Verdeguer F, Liesa M, Cunningham JT, Vogel RO, Chim H, Liu H, Romanino K, Shirihai OS, Vazquez F, Ruegg MA, Shi Y, Puigserver P (2012) Defective mitochondrial morphology and bioenergetic function in mice lacking the transcription factor Yin Yang 1 in skeletal muscle. *Mol Cell Biol* 32: 3333–3346
- Borensztein M, Monnier P, Court F, Louault Y, Ripoche MA, Turet L, Yao Z, Tapscott SJ, Forne T, Montarras D, Dandolo L (2013) Myod and H19-Igf2 locus interactions are required for diaphragm formation in the mouse. *Development* 140: 1231–1239
- Buckingham M (2007) Skeletal muscle progenitor cells and the role of Pax genes. *C R Biol* 330: 530–533
- Buckingham M, Relaix F (2007) The role of Pax genes in the development of tissues and organs: Pax3 and Pax7 regulate muscle progenitor cell functions. *Annu Rev Cell Dev Biol* 23: 645–673
- Bulfield G, Siller WG, Wight PA, Moore KJ (1984) X chromosome-linked muscular dystrophy (mdx) in the mouse. *Proc Natl Acad Sci USA* 81: 1189–1192
- Caretti G, Di Padova M, Micales B, Lyons GE, Sartorelli V (2004) The Polycomb Ezh2 methyltransferase regulates muscle gene expression and skeletal muscle differentiation. *Genes Dev* 18: 2627–2638
- Chen H, Chan DC (2017) Mitochondrial dynamics in regulating the unique phenotypes of cancer and stem cells. *Cell Metab* 26: 39–48
- Chen X, He L, Zhao Y, Li Y, Zhang S, Sun K, So K, Chen F, Zhou L, Lu L, Wang L, Zhu X, Bao X, Esteban MA, Nakagawa S, Prasanth KV, Wu Z, Sun H, Wang H (2017) Malat1 regulates myogenic differentiation and muscle regeneration through modulating MyoD transcriptional activity. *Cell Discov* 3: 17002
- Cheung TH, Quach NL, Charville GW, Liu L, Park L, Edalati A, Yoo B, Hoang P, Rando TA (2012) Maintenance of muscle stem-cell quiescence by microRNA-489. *Nature* 482: 524–528
- Cunningham JT, Rodgers JT, Arlow DH, Vazquez F, Mootha VK, Puigserver P (2007) mTOR controls mitochondrial oxidative function through a YY1-PGC-1 $\alpha$  transcriptional complex. *Nature* 450: 736–740
- Diao Y, Guo X, Li Y, Sun K, Lu L, Jiang L, Fu X, Zhu H, Sun H, Wang H, Wu Z (2012) Pax3/7BP is a Pax7- and Pax3-binding protein that regulates the proliferation of muscle precursor cells by an epigenetic mechanism. *Cell Stem Cell* 11: 231–241
- Donohoe ME, Zhang X, McGinnis L, Biggers J, Li E, Shi Y (1999) Targeted disruption of mouse Yin Yang 1 transcription factor results in peri-implantation lethality. *Mol Cell Biol* 19: 7237–7244
- Esteban MA, Tran MG, Harten SK, Hill P, Castellanos MC, Chandra A, Raval R, O'Brien TS, Maxwell PH (2006) Regulation of E-cadherin expression by VHL and hypoxia-inducible factor. *Cancer Res* 66: 3567–3575

- Garcia-Prat L, Sousa-Victor P, Munoz-Canoves P (2017) Proteostatic and metabolic control of stemness. *Cell Stem Cell* 20: 593–608
- Gibson GE, Thakkar A (2018) Mitochondria/metabolic reprogramming in the formation of neurons from peripheral cells: cause or consequence and the implications to their utility. *Neurochem Int* 117: 65–76
- Gordon S, Akopyan G, Garban H, Bonavida B (2006) Transcription factor YY1: structure, function, and therapeutic implications in cancer biology. *Oncogene* 25: 1125–1142
- He Y, Casaccia-Bonnel P (2008) The Yin and Yang of YY1 in the nervous system. *J Neurochem* 106: 1493–1502
- Hutcheson DA, Zhao J, Merrell A, Haldar M, Kardon G (2009) Embryonic and fetal limb myogenic cells are derived from developmentally distinct progenitors and have different requirements for beta-catenin. *Genes Dev* 23: 997–1013
- Ito K, Suda T (2014) Metabolic requirements for the maintenance of self-renewing stem cells. *Nat Rev Mol Cell Biol* 15: 243–256
- Juan AH, Derfoul A, Feng X, Ryall JG, Dell'Orso S, Pasut A, Zare H, Simone JM, Rudnicki MA, Sartorelli V (2011) Polycomb EZH2 controls self-renewal and safeguards the transcriptional identity of skeletal muscle stem cells. *Genes Dev* 25: 789–794
- Keller C, Hansen MS, Coffin CM, Capecchi MR (2004) Pax3: Fkhr interferes with embryonic Pax3 and Pax7 function: implications for alveolar rhabdomyosarcoma cell of origin. *Genes Dev* 18: 2608–2613
- Kim D, Perteau G, Trapnell C, Pimentel H, Kelley R, Salzberg SL (2013) TopHat2: accurate alignment of transcriptomes in the presence of insertions, deletions and gene fusions. *Genome Biol* 14: R36
- Kleiman E, Jia H, Loguercio S, Su AI, Feeney AJ (2016) YY1 plays an essential role at all stages of B-cell differentiation. *Proc Natl Acad Sci USA* 113: E3911–E3920
- Langmead B, Salzberg SL (2012) Fast gapped-read alignment with Bowtie 2. *Nat Methods* 9: 357–359
- Lepper C, Conway SJ, Fan CM (2009) Adult satellite cells and embryonic muscle progenitors have distinct genetic requirements. *Nature* 460: 627–631
- Lu L, Zhou L, Chen EZ, Sun K, Jiang P, Wang L, Su X, Sun H, Wang H (2012) A Novel YY1-miR-1 regulatory circuit in skeletal myogenesis revealed by genome-wide prediction of YY1-miRNA network. *PLoS One* 7: e27596
- Lu L, Sun K, Chen X, Zhao Y, Wang L, Zhou L, Sun H, Wang H (2013) Genome-wide survey by ChIP-seq reveals YY1 regulation of lincRNAs in skeletal myogenesis. *EMBO J* 32: 2575–2588
- Merrell AJ, Kardon G (2013) Development of the diaphragm – a skeletal muscle essential for mammalian respiration. *FEBS J* 280: 4026–4035
- Mousavi K, Zare H, Wang AH, Sartorelli V (2012) Polycomb protein Ezh1 promotes RNA polymerase II elongation. *Mol Cell* 45: 255–262
- Palacios D, Mozzetta C, Consalvi S, Caretti G, Saccone V, Proserpio V, Marquez VE, Valente S, Mai A, Forcales SV, Sartorelli V, Puri PL (2010) TNF/p38alpha/polycomb signaling to Pax7 locus in satellite cells links inflammation to the epigenetic control of muscle regeneration. *Cell Stem Cell* 7: 455–469
- Peng XL, So KK, He L, Zhao Y, Zhou J, Li Y, Yao M, Xu B, Zhang S, Yao H, Hu P, Sun H, Wang H (2017) MyoD- and FoxO3-mediated hotspot interaction orchestrates super-enhancer activity during myogenic differentiation. *Nucleic Acids Res* 45: 8785–8805
- Perekatt AO, Valdez MJ, Davila M, Hoffman A, Bonder EM, Gao N, Verzi MP (2014) YY1 is indispensable for Lgr5 + intestinal stem cell renewal. *Proc Natl Acad Sci USA* 111: 7695–7700
- Relaix F, Zammit PS (2012) Satellite cells are essential for skeletal muscle regeneration: the cell on the edge returns centre stage. *Development* 139: 2845–2856
- Ryall JG, Dell'Orso S, Derfoul A, Juan A, Zare H, Feng X, Clermont D, Koulnis M, Gutierrez-Cruz G, Fulco M, Sartorelli V (2015) The NAD(+)-dependent SIRT1 deacetylase translates a metabolic switch into regulatory epigenetics in skeletal muscle stem cells. *Cell Stem Cell* 16: 171–183
- Sambasivan R, Gayraud-Morel B, Dumas G, Cimper C, Paisant S, Kelly RG, Tajbakhsh S (2009) Distinct regulatory cascades govern extraocular and pharyngeal arch muscle progenitor cell fates. *Dev Cell* 16: 810–821
- Schell JC, Wisidagama DR, Bensard C, Zhao H, Wei P, Tanner J, Flores A, Mohlman J, Sorensen LK, Earl CS, Olson KA, Miao R, Waller TC, Delker D, Kanth P, Jiang L, DeBerardinis RJ, Bronner MP, Li DY, Cox JE et al (2017) Control of intestinal stem cell function and proliferation by mitochondrial pyruvate metabolism. *Nat Cell Biol* 19: 1027–1036
- Seale P, Sabourin LA, Girgis-Gabardo A, Mansouri A, Gruss P, Rudnicki MA (2000) Pax7 is required for the specification of myogenic satellite cells. *Cell* 102: 777–786
- Skapek SX, Rhee J, Kim PS, Novitch BG, Lassar AB (1996) Cyclin-mediated inhibition of muscle gene expression via a mechanism that is independent of pRB hyperphosphorylation. *Mol Cell Biol* 16: 7043–7053
- Tang AH, Rando TA (2014) Induction of autophagy supports the bioenergetic demands of quiescent muscle stem cell activation. *EMBO J* 33: 2782–2797
- Trapnell C, Roberts A, Goff L, Pertea G, Kim D, Kelley DR, Pimentel H, Salzberg SL, Rinn JL, Pachter L (2012) Differential gene and transcript expression analysis of RNA-seq experiments with TopHat and Cufflinks. *Nat Protoc* 7: 562–578
- Wan M, Huang W, Kute TE, Miller LD, Zhang Q, Hatcher H, Wang J, Stovall DB, Russell GB, Cao PD, Deng Z, Wang W, Zhang Q, Lei M, Torti SV, Akman SA, Sui G (2012) Yin Yang 1 plays an essential role in breast cancer and negatively regulates p27. *Am J Pathol* 180: 2120–2133
- Wang H, Hertlein E, Bakkar N, Sun H, Acharyya S, Wang J, Carathers M, Davuluri R, Guttridge DC (2007) NF-kappaB regulation of YY1 inhibits skeletal myogenesis through transcriptional silencing of myofibrillar genes. *Mol Cell Biol* 27: 4374–4387
- Wang H, Garzon R, Sun H, Ladner KJ, Singh R, Dahlman J, Cheng A, Hall BM, Qualman SJ, Chandler DS, Croce CM, Guttridge DC (2008) NF-kappaB-YY1-miR-29 regulatory circuitry in skeletal myogenesis and rhabdomyosarcoma. *Cancer Cell* 14: 369–381
- Wang L, Zhou L, Jiang P, Lu L, Chen X, Lan H, Guttridge DC, Sun H, Wang H (2012) Loss of miR-29 in myoblasts contributes to dystrophic muscle pathogenesis. *Mol Ther* 20: 1222–1233
- Wang G, Zhu H, Situ C, Han L, Yu Y, Cheung TH, Liu K, Wu Z (2018) p110alpha of PI3K is necessary and sufficient for quiescence exit in adult muscle satellite cells. *EMBO J* 37: e98239
- Wu S, Kasim V, Kano MR, Tanaka S, Ohba S, Miura Y, Miyata K, Liu X, Matsuhashi A, Chung UI, Yang L, Kataoka K, Nishiyama N, Miyagishi M (2013) Transcription factor YY1 contributes to tumor growth by stabilizing hypoxia factor HIF-1alpha in a p53-independent manner. *Cancer Res* 73: 1787–1799
- Wu S, Wang H, Li Y, Xie Y, Huang C, Zhao H, Miyagishi M, Kasim V (2018) Transcription factor YY1 promotes cell proliferation by directly activating the pentose phosphate pathway. *Can Res* 78: 4549–4562
- Xie L, Yin A, Nichenko AS, Beedle AM, Call JA, Yin H (2018) Transient HIF2A inhibition promotes satellite cell proliferation and muscle regeneration. *J Clin Invest* 128: 2339–2355
- Yang X, Yang S, Wang C, Kuang S (2017) The hypoxia-inducible factors HIF1alpha and HIF2alpha are dispensable for embryonic muscle development but essential for postnatal muscle regeneration. *J Biol Chem* 292: 5981–5991

- Zhang Y, Liu T, Meyer CA, Eeckhoute J, Johnson DS, Bernstein BE, Nusbaum C, Myers RM, Brown M, Li W, Liu XS (2008) Model-based analysis of CHIP-Seq (MACS). *Genome Biol* 9: R137
- Zhang ZK, Li J, Liu J, Guo B, Leung A, Zhang G, Zhang BT (2016) Icaritin requires Phosphatidylinositol 3 kinase (PI3K)/Akt signaling to counteract skeletal muscle atrophy following mechanical unloading. *Sci Rep* 6: 20300
- Zhou L, Wang L, Lu L, Jiang P, Sun H, Wang H (2012a) Inhibition of miR-29 by TGF-beta-Smad3 signaling through dual mechanisms promotes transdifferentiation of mouse myoblasts into myofibroblasts. *PLoS One* 7: e33766
- Zhou L, Wang L, Lu L, Jiang P, Sun H, Wang H (2012b) A novel target of microRNA-29, Ring1 and YY1-binding protein (Rybp), negatively regulates skeletal myogenesis. *J Biol Chem* 287: 25255–25265
- Zhou L, Sun K, Zhao Y, Zhang S, Wang X, Li Y, Lu L, Chen X, Chen F, Bao X, Zhu X, Wang L, Tang LY, Esteban MA, Wang CC, Jauch R, Sun H, Wang H (2015) Linc-YY1 promotes myogenic differentiation and muscle regeneration through an interaction with the transcription factor YY1. *Nat Commun* 6: 10026
- Zhu H, Xiao F, Wang G, Wei X, Jiang L, Chen Y, Zhu L, Wang H, Diao Y, Wang H, Ip NY, Cheung TH, Wu Z (2016) STAT3 regulates self-renewal of adult muscle satellite cells during injury-induced muscle regeneration. *Cell Rep* 16: 2102–2115